Politecnico di Torino

Master's Degree in Mathematical Engineering

Theoretical analysis and numerical simulation in discrete fracture networks using both the virtual element method and the mortar method

Candidate:
Lorenzo Neva, mat. 313795

Supervisor:
Prof. Fabio Vicini

Academic year 2023/2024

Contents

Introduction

The Discrete Fracture Network (DFN) method is a discrete modeling approach designed to simulate fluid flow and transport phenomena within fractured rock formations. Developed in the 1980s [22], this technique has been refined and expanded to address both 2D and 3D situations. Over the years, it has seen extensive application in various fields, including civil, environmental, and reservoir engineering, as well as other areas of geoscience and geoengineering.
In this method, fractures are represented as 2D planar domains, with fluid flow restricted to the fractures themselves, as the surrounding rock matrix is considered impermeable. A central challenge in these simulations is the geometric handling of the domain, particularly when global or local mesh conformity is necessary. Given a DFN Ω, a set of N open planar polygons F_i, $i = 1, \dots, N$, where each one represents a fracture, the challenging part to deal with is the intersections between the F_i, called traces and denoted by S. On the domain Ω, Darcy's law is adopted as a model for the equilibrium of the hydraulic head H, which is solved on each fracture: this equation is coupled with the balance of fluxes on traces and by continuity of the solution across traces.
Problems of this kind can be addressed from an analytical-computational perspective using the Virtual Element Method (VEM), introduced in [5, 6]. This is a highly adaptable mesh-based technique that allows for the use of general polygonal and polyhedral meshes, including non-convex, degenerate, and non-matching elements. Notably, VEM can produce highly regular solutions, making it more suitable than traditional finite element methods (FEM) for solving higher-order problems and approximating eigenvalues. The key advantages of VEM are its solid mathematical foundation, computational efficiency and accuracy. Another approach that can be adopted is the Mortar Method, a domain decomposition method introduced in [13, 14], which allows for non-matching meshes at fracture interfaces and is particularly useful in multi-physics problems.
These methods offer two distinct computational approaches: a fully conforming VEM and a mixed VEM-Mortar method, which differ in their handling of conditions on the traces. Depending on the user's preference for either as a fully VEM or Mortar approach, continuity will be enforced strongly in the former case (see [11]) and weakly in the latter one (see [10]).
This aspect is strongly linked to the discretization of the domain. Initially, a good quality mesh of convex polygons, with an arbitrary number of sides, is created for each fracture F_i. A fully VEM approach leads to the creation of a new mesh, locally and globally conforming to the traces of the fractures, called the VEM mesh (procedure illustrated in [10]). In this case, the discretization of the traces must take into account the discretization in the respective fractures,

effectively adding discrete points. On the other hand, the Mortar method allows the independent discretization of fractures since an integral condition must be solved on the traces rather than a point one.
Each method has its own pros and cons: the use of *Mortar traces*, i.e. traces where a weak continuity condition is imposed, simplifies the geometric aspect of the implementation but leads to an increase in the linear system conditioning and dimensions, namely a saddle point problem. On the other hand, the use of *VEM traces* offers clear advantages in terms of the discrete spaces involved but necessitates the creation of conforming meshes between fractures.

The thesis has two primary objectives. First, it undertakes a theoretical analysis of the problem, detailing both methods and their coupling. The innovative contribution here lies in the combined use of these methods to achieve well-posedness of the discrete problem and an a-priori error estimate for the discretization. The thesis also provides a detailed implementation guide, with a particular focus on the matrices involved in the saddle-point problem that emerges. The second objective is the application of the mixed VEM-Mortar method to a benchmark problem. Starting from a C++ code developed for a fully VEM approach, I incorporate in the code the mixed VEM-Mortar method implementation. This work lays the foundation for future research aimed at studying how the error behavior and matrix condition number in the saddle-point problem vary with the number of VEM or Mortar traces used.
The thesis is structured as follows: the next chapter provides a basic introduction to the problem where most of the notation that will be used in the following chapters will be introduced. Chapter 2 contains a description of the VEM method: various possibilities for the introduced spaces and bilinear forms will be analyzed, comparing them with those used in the literature cited in the bibliography. Using [29], the Mortar method will be presented in Chapter 3, together with the Mortar formulation of the problem and some theoretical results, such as an a priori estimate. In the concluding chapter, after a brief paragraph dedicated to implementation of the method and its matrix formulation, the numerical results will be shown.

Chapter 1

Description of the problem

1.1 Geometric description and notation

A Discrete Fracture Network (DFN) model is a 3D domain $\Omega := \bigcup_{i=1}^{N} F_i$, where each fracture is represented by a planar polygon $F_i \subset \mathbb{R}^2, i = 1, \ldots, N$. Let us denote by ∂F_i the boundary of F_i and by $\partial\Omega$ the set of all the fracture boundaries, $\partial\Omega = \cup_{i=1}^{N} \partial F_i$. Let Γ^D be a non-empty portion of the border of Ω denoting the Dirichlet boundary. Same for Γ^N denoting the Neumann boundary. Let us assume $\partial\Omega = \Gamma^D \cup \Gamma^N$ with $\Gamma^D \cap \Gamma^N = \emptyset$. The boundary of each fracture is divided into a Dirichlet part $\Gamma_i^D = \Gamma^D \cap \partial F_i$ and a Neumann part $\Gamma_i^N = \Gamma^N \cap \partial F_i$. An empty Dirichlet boundary, $\Gamma_i^D = \emptyset$ is allowed on some fractures. Intersections between fractures are called traces and are denoted by S, whit $\mathcal{S}$ representing the set of all fractures. For each $S \in \mathcal{S}$, it is convenient to identify the set $\mathcal{I}_S = \{i, j\}$ of the indices of the two fractures, namely F_i, F_j, intersecting at S and $\mathcal{S}_i = \{\, S \in \mathcal{S} : i \in \mathcal{I}_S \,\}$.
The following assumptions are made for the DFN:

- $\bar{\Omega}$ is a connected set;
- each trace $S \in \mathcal{S}$ is shared by exactly two polygonal fractures F_i and F_j, $i \neq j : S \subseteq \bar{F}_i \cap \bar{F}_j$. This is made possible by dividing the intersecting traces into subtraces;
- on each fracture, the transmissivity tensor $\mathbf{K}_i$ is symmetric and uniformly positive definite. Let's assume that the value $\mathbf{K}_i$ is constant over the entire fracture F_i.

In the remainder of this chapter and in the following ones, notation $(\cdot, \cdot)_E$ will denote the L^2-scalar product on the domain E, $\|\cdot\|_E$ the L^2-norm on E and $|\cdot|_{1,E}$ the $H^1(E)$-seminorm; the duality product between $H^{-\alpha}(\omega)$ and $H^{\alpha}(\omega)$ is indicated as $\langle \cdot, \cdot \rangle_{\pm\alpha,\omega}$, while the superscript $(A)'$ indicates the dual space of the space A. The symbol $\gamma_E(\cdot)$ denotes the trace operators on E.

1.2 Model description

The quantity of interest is the hydraulic head H that can be evaluated in Ω by means of Darcy's law. As defined in [1], H is composed by the fluid pressure

$P = p/(\rho g)$, g is the gravitational constant, ρ the fluid density, plus ζ, the elevation with respect to a reference point:

$$H = P + \zeta.$$

The Dirichlet boundary condition imposed on Γ^D is denoted by $H^D \in H^{\frac{1}{2}}(\Gamma^D)$, and its restriction on a generic Γ_i^D is called $H_i^D \in H^{\frac{1}{2}}(\Gamma_i^D)$. Similarly, let $H^N \in H^{-\frac{1}{2}}(\Gamma^N)$ denote the Neumann boundary condition, and its restriction on a generic Γ_i^N is called $H_i^N \in H^{-\frac{1}{2}}(\Gamma_i^N)$.

Given the trace operator on Γ_i^D, that is $\gamma_{\Gamma_i^D} : \mathrm{H}^1(F_i) \to \mathrm{H}^{\frac{1}{2}}\left(\Gamma_i^D\right)$, let's define the following functional spaces:

$$\begin{aligned}
V_i &= \left\{ v \in \mathrm{H}^1(F_i) : \gamma_{\Gamma_i^D}(v) = 0 \right\} \quad \forall i = 1, \ldots, N, \\
V_i^D &= \left\{ v \in \mathrm{H}^1(F_i) : \gamma_{\Gamma_i^D}(v) = H_i^D \right\} \quad \forall i = 1, \ldots, N, \\
V^D &= \prod_{i=1}^{N} V_i^D, \quad V = \prod_{i=1}^{N} V_i.
\end{aligned}$$

In general, a function $v \in H^1(F_i)$ has its trace in $H^{\frac{1}{2}}(\partial F_i)$ and the normal component of its flux is in the dual space $H^{-\frac{1}{2}}(\partial F_i)$.

Darcy's law gives rise to an elliptic Dirichlet/Neumann problem. As it is typically done in this type of problems, the solution is decomposed into two parts $H = H_0 + R^D$, where $H \in V^D$, $H_0 \in V$, and R^D represents the Dirichlet data in the following sense:

$$\forall i = 1, \ldots, N, \quad R_i^D := R^D|_{F_i} \quad \text{is such that} \quad \gamma_{\Gamma_i^D}(R_i^D) = H_i^D.$$

The source term is represented by $f \in L^2(\Omega)$. Moreover, $H_i \in V_i^D, H_{0i} \in V_i, f_i \in L^2(F_i)$ and $v_i \in V_i$ are the restrictions in the fracture F_i of H, H_0, f and an arbitrary $v \in V$, $\forall i = 1, \ldots, N$.
In addition, let's define $\mathbf{n}_S^i$ as the unit vector normal to trace S on fracture F_i. The notation

$$\frac{\partial H_i}{\partial \mathbf{n}_S^i} = \mathbf{n}_S^i \cdot \nabla H_i \in H^{\frac{1}{2}}(S)$$

represents the outward co-normal derivative of the hydraulic head. The symbol $\left[\!\left[K_i \frac{\partial H_i}{\partial \mathbf{n}_S^i} \right]\!\right]_S$ denotes the jump of the co-normal derivative of H_i across S on F_i, that belongs to the dual space $H^{-\frac{1}{2}}(S) = \left(H_{00}^{\frac{1}{2}}(S)\right)'$. See [27], page 342, for the definition of this trace space.
Finally, Darcy's law applied to the fracture F_i can be formulated:

$$\begin{aligned}
(K_i \nabla H_{0i}, \nabla v_i)_{F_i} - \sum_{S \in \mathcal{S}_i} \left\langle \left[\!\left[K_i \frac{\partial H_i}{\partial \mathbf{n}_S^i} \right]\!\right]_S, \gamma_S(v_i) \right\rangle_{\pm\frac{1}{2}, S} &= (f_i, v_i)_{F_i} + \\
\left\langle H_i^N, \gamma_{\Gamma_i^N}(v_i) \right\rangle_{\pm\frac{1}{2}, \Gamma_i^N} - \left(K_i \nabla R_i^D, \nabla v_i\right)_{F_i}&.
\end{aligned} \tag{1.1}$$

The previous equation must be coupled by :

- the balance of fluxes on traces

$$\forall S \in \mathcal{S}, \text{ if } \mathcal{I}_S = \{i, j\}, \quad \left[\!\left[K_i \frac{\partial H_i}{\partial \mathbf{n}_S^i} \right]\!\right]_S + \left[\!\left[K_j \frac{\partial H_j}{\partial \mathbf{n}_S^j} \right]\!\right]_S = 0; \tag{1.2}$$

- the second condition varies depending on the trace under consideration. It is necessary to impose the continuity of the solution along the traces, but this can be a point-wise (or strong) condition or an integral (or weak) one. As anticipated in the introductory section, the unique aspect of this work lies precisely in starting from a hybrid approach as in [10], while considering the possibility of requiring strong continuity along certain traces, which are called *VEM traces* traces, distinguishing them from traces where weak continuity, called *Mortar traces*, is imposed. The sets containing *VEM traces* and *Mortar traces*, respectively, are $\mathcal{S}_V$ and $\mathcal{S}_M$.
  The two conditions are:

$$H_i|_S - H_j|_S = 0, \quad \text{if } \mathcal{I}_S = \{i, j\}, \quad \forall S \in \mathcal{S}_V, \tag{1.3}$$

  or

$$\forall \psi \in \mathrm{H}^{-\frac{1}{2}}(S), \quad \langle [\![H]\!]_S, \psi \rangle_{\pm\frac{1}{2},S} = 0, \quad \forall S \in \mathcal{S}_M. \tag{1.4}$$

  The first condition can also be written as $[\![H]\!]_S = 0$.

Remark 1. *Regarding the existence and uniqueness of the solution, the theoretical treatment is conducted for a saddle-point problem arising from the coupling of VEM and Mortar with a weak continuity condition imposed everywhere ($\mathcal{S}_M \equiv \mathcal{S}$), as in [10]. The global DOFs chosen in the VEM settings authorize to manage two different fractures that share a VEM trace as an single fracture.*

For the remainder of the chapter, all traces will be Mortar unless explicitly stated otherwise. For all $S \in \mathcal{S}$, the bilinear form $b_S : V^D \times H^{-\frac{1}{2}}(S) \to \mathbb{R}$ is defined as

$$b_S(v, \psi) = \langle [\![v]\!]_S, \psi \rangle_{\pm\frac{1}{2},S}, \tag{1.5}$$

so it's possible to redefine (1.4) as

$$\forall S \in \mathcal{S}, \ \forall \psi \in H^{-\frac{1}{2}}(S), \quad b_S(H, \psi) = 0. \tag{1.6}$$

It is useful to define a function that maps indices of the fractures forming a trace, in order to more precisely express the jump of a function across it. Let $\mathcal{I}_S = \{\, i, j \,\}$, then

$$m_S : \mathcal{I}_S \to \{0, 1\}, \qquad m_S(k) = \begin{cases} 1 & \text{if } k = \min\{i, j\}, \\ 0 & \text{otherwise.} \end{cases} \tag{1.7}$$

Due to this, it is possible to write that

$$\forall v \in V^D, \forall S \in \mathcal{S}, \quad [\![v]\!]_S = \sum_{i \in \mathcal{I}_S} (-1)^{m_S(i)} \gamma_S(v_i).$$

Here's the global space of Lagrange multipliers

$$M = \prod_{S \in \mathcal{S}} H^{-\frac{1}{2}}(S),$$

and for every function in such a space $\Lambda \in M$, for all $S \in \mathcal{S}$:

$$\Lambda|_S := \Lambda_S = \left[\!\left[K_i \frac{\partial H}{\partial n_i} \right]\!\right]_S . \tag{1.8}$$

where i is such that $m_S(i) = 1$, in order to have a unique definition.

Let's define a bilinear form similar to the previous one (1.5), but defined on each fracture.

$$b_i : V_i^D \times M \to \mathbb{R}, \quad b_i(v_i, \psi) = \sum_{S \in \mathcal{S}_i} (-1)^{m_S(i)} \langle \gamma_S(v_i), \psi \rangle_{-\frac{1}{2},S}. \tag{1.9}$$

In order to obtain the saddle-point form from (1.1), let's introduce a bilinear form on each fracture $a_i : V_i \times V_i \to \mathbb{R}$ as

$$a_i(u_i, v_i) = (K_i \nabla u_i, \nabla v_i)_{F_i}, \quad \forall i = 1, \dots, N,$$

and, finally (1.1) is equivalent to:

$$a_i(H_{0i}, v_i) + b_i(v_i, \Lambda) = (f_i, v_i)_{F_i} + \left\langle H_i^N, v_i \right\rangle_{\pm\frac{1}{2},\Gamma_i^N} - a_i(R_i^D, v_i), \quad \forall v \in V. \tag{1.10}$$

In view of a global formulation of the problem, it is useful to define

$$a : V \times V \to \mathbb{R}, \qquad a(u, v) = \sum_{i=1}^{N} a_i(u_i, v_i), \quad \forall u, v \in V, \tag{1.11}$$

and

$$b : V^D \times M \to \mathbb{R}, \qquad b(v, \psi) = \sum_{i=1}^{N} b_i(v_i, \psi), \quad \forall v \in V^D, \forall \psi \in M.$$

Using both definitions of the two different bilinear form related to $b(\cdot, \cdot)$, respectively $b_i(\cdot, \cdot)$ and $b_S(\cdot, \cdot)$, from (1.6) the following is obtained:

$$b(H, \psi) = \sum_{S \in \mathcal{S}} b_S(H, \psi) = 0, \quad \forall \psi \in H^{-\frac{1}{2}}(S). \tag{1.12}$$

Remark 2. *To obtain the previous result, the subsequent step was implicitly taken:*

$$\sum_{S \in \mathcal{S}} b_S(H, \psi) = \sum_{i=1}^{N} b_i(H, \psi)$$

Here's the proof for a DFN like Figure 1.1, where $\mathcal{S}_1 = \{ S_1, S_3 \}$, $\mathcal{S}_2 = \{ S_1, S_2 \}$ *and* $\mathcal{S}_3 = \{ S_2, S_3 \}$. *The notation will be reduced from* $\langle \cdot, \cdot \rangle_{-\frac{1}{2},S}$ *to* $\langle \cdot, \cdot \rangle_S$ *for*

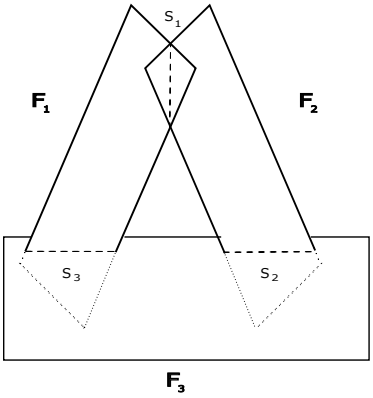

Figure 1.1: Example of DFN with only 3 fractures.

simplicity. For all $v \in V^D$ *and* $\psi \in M$,

$$\begin{aligned}
\sum_{i=1}^{N} b_i(v,\psi) &= \sum_{i=1}^{N} \sum_{S\in\mathcal{S}_i} (-1)^{m_S(i)} \langle \gamma_S(v_i), \psi\rangle_S = \\
&= \sum_{S\in\mathcal{S}_1} (-1)^{m_S(1)} \langle \gamma_S(v_1), \psi\rangle_S + \sum_{S\in\mathcal{S}_2} (-1)^{m_S(2)} \langle \gamma_S(v_2), \psi\rangle_S \\
&\quad + \sum_{S\in\mathcal{S}_3} (-1)^{m_S(3)} \langle \gamma_S(v_3), \psi\rangle_S \\
&= (-1)^{m_{S_1}(1)} \langle \gamma_{S_1}(v_1), \psi\rangle_{S_1} + (-1)^{m_{S_3}(1)} \langle \gamma_{S_3}(v_1), \psi\rangle_{S_3} \\
&\quad + (-1)^{m_{S_1}(2)} \langle \gamma_{S_1}(v_2), \psi\rangle_{S_1} + (-1)^{m_{S_2}(2)} \langle \gamma_{S_2}(v_2), \psi\rangle_{S_2} \\
&\quad + (-1)^{m_{S_2}(3)} \langle \gamma_{S_2}(v_3), \psi\rangle_{S_2} + (-1)^{m_{S_3}(3)} \langle \gamma_{S_3}(v_3), \psi\rangle_{S_3} \\
&= -\langle \gamma_{S_1}(v_1), \psi\rangle_{S_1} - \langle \gamma_{S_3}(v_1), \psi\rangle_{S_3} + \langle \gamma_{S_1}(v_2), \psi\rangle_{S_1} \\
&\quad - \langle \gamma_{S_2}(v_2), \psi\rangle_{S_2} + \langle \gamma_{S_2}(v_3), \psi\rangle_{S_2} + \langle \gamma_{S_3}(v_3), \psi\rangle_{S_3} \\
&= \sum_{i\in I_{S_1}} (-1)^{m_{S_1}(i)} \langle \gamma_{S_1}(v_i), \psi\rangle_{S_1} + \sum_{i\in I_{S_2}} (-1)^{m_{S_2}(i)} \langle \gamma_{S_2}(v_i), \psi\rangle_{S_2} \\
&\quad + \sum_{i\in I_{S_3}} (-1)^{m_{S_3}(i)} \langle \gamma_{S_3}(v_i), \psi\rangle_{S_3} \\
&= \sum_{S\in\mathcal{S}} b_s(v,\psi).
\end{aligned}$$

Finally, the following saddle-point problem is obtained by summing the equation (1.10) over all the fractures and by (1.12):

$$\begin{cases} a(H_0, v) + b(v, \Lambda) = (f, v) + \left\langle H^N, v \right\rangle_{\pm\frac{1}{2},\Gamma^N} - a(R^D, v) & \forall v \in V, \\ b(H_0, \psi) = -b(R^D, \psi) & \forall \psi \in M. \end{cases} \tag{1.13}$$

The norm defined below is used on V^D and V:

$$\|v\|_V = \left(\sum_{i=1}^{N} \|v_i\|^2_{L^2(F_i)} + a_i(v_i, v_i) \right)^{\frac{1}{2}}. \tag{1.14}$$

Well-posedness of (1.13) follows observing that, introducing the Hilbert space as in [10]

$$W = \left\{ v \in V : \forall S \in S, \forall \psi \in H^{-\frac{1}{2}}(S), \quad \langle [\![v]\!]_S, \psi \rangle_{\pm\frac{1}{2},S} = 0 \right\} = \ker(b),$$

the system (1.13) is equivalent to: find $H_0 \in W$ such that

$$a(H_0, v) = (f, v) + \left\langle H^N, v \right\rangle_{\pm\frac{1}{2},\Gamma^N} - a(R^D, v) \quad \forall v \in W. \tag{1.15}$$

Remark 3. *The use of W is essential because it ensures that the condition of balance of fluxes on traces* (1.2) *is automatically satisfied.*

Chapter 2

The Virtual Element Method

The Virtual Element Method (VEM) [8] can be viewed as an extension of FEM to general polygonal elements, firstly introduced in [5, 6]. The key strengths of the VEM are its solid mathematical foundation, ease of implementation, computational efficiency and precision. This method has been utilized in elasticity problems [18], plate bending [17], Navier-Stokes [19] and the Stokes problem [3], and it has also generated interest in various other applications. The characteristic of allowing polygonal elements it's optimal for problems in the DFN framework [10, 11]. An important feature of the VEM method is that it utilizes discrete functional spaces equipped with non-polynomial functions. Unlike in the FEM framework, these spaces include functions whose explicit form is unknown; it is sufficient to know their value at a certain set of degrees of freedom. From an implementation perspective, VEM involves more effort compared to FEM when constructing elemental matrices: this is due to the fact that the basis functions are not known analytically.
Section 2.1 introduces all the objects related to the VEM that will be used in Section 2.2, where the method is applied to DNF context.

Following the construction of the local discrete spaces as outlined in [6], it is appropriate to introduce the scaled moments for any polygonal domain D in $\mathbb{R}^2$. Let $\boldsymbol{x}_D$ and h_D be the centroid and the diameter of D, respectively, $\mathbb{P}_k(D)$ will be defined as the space of polynomials of degree less or equal than $k \geq 1$ in D. A multi-index $\boldsymbol{\alpha} = (\alpha_1, \alpha_2)$ allows the introduction of scaled monomial $m_{\boldsymbol{\alpha}}$ of degree equal to $|\boldsymbol{\alpha}| = \alpha_1 + \alpha_2$:

$$m_{\boldsymbol{\alpha}}(\boldsymbol{x}) := \left(\frac{\boldsymbol{x} - \boldsymbol{x}_{\mathcal{D}}}{h_{\mathcal{D}}} \right)^{\boldsymbol{\alpha}}, \tag{2.1}$$

for all $\boldsymbol{x} \in D$. $\mathcal{M}_k(\mathcal{D})$ is the set of scaled monomials of degree less than or equal to k :

$$\mathcal{M}_k(D) := \{ m_{\boldsymbol{\alpha}} : 0 \leq |\boldsymbol{\alpha}| \leq k \},$$

and it's easy to check that this set is a basis for $\mathbb{P}_k(D)$. The monomials are ordered as in Table 2.1.

i	1	2	3	4	5	6
$\boldsymbol{\alpha}$	(0,0)	(1,0)	(0,1)	(2,0)	(1,1)	(0,2)
k	0	1	1	2	2	2

Table 2.1: $2D$ monomials exponents ordering for $k \leq 2$.

2.1 Basis of the Virtual Element Method

Let's consider a fracture $F_i \subset \mathbb{R}^2$ and a mesh $\tau_{\delta,i}$ on F_i made of a finite number of convex polygons E with mesh parameter δ (i.e. the square root of the maximum element area). Let's remark that all the polygons are convex for simplicity: in general, the VEM can include also non-convex polygons, but it's not the case of interest in this context. For $k \geq 1$, the original local virtual element space $V_{k,\delta}^{\text{old}}(E)$ is defined in [5, 6] as

$$V_{k,\delta}^{\text{old}}(E) = \left\{ v_\delta \in \mathrm{H}^1(E) : v_{\delta|\partial E} \in C^0(\partial E), v_{\delta|e} \in \mathbb{P}_k(e), \forall e \subset \partial E \right. \\ \left. \Delta v_\delta \in \mathbb{P}_{k-2}(E) \right\}, \tag{2.2}$$

where ∂E indicates the boundary of E and e is an edge on that boundary. If $k < 2$, $\mathbb{P}_{-1}(E) \equiv \{0\}$. It's not difficult to check that $V_{k,\delta}^{\text{old}}(E)$ contains all polynomial of degree k, i.e. $\mathbb{P}_k(E) \subset V_{k,\delta}^{\text{old}}(E)$, plus other non-polynomial functions.
Referring back to the description in [5], there exist a unique function $v_\delta \in H^1(E)$ for every given $q_{k-2} \in \mathbb{P}_{k-2}(E)$ and $g \in C^0(\partial E) : g_{|e} \in \mathbb{P}_k(e) \quad \forall e \subset \partial E$ such that:

$$\Delta v_\delta = q_{k-2}, \qquad v_\delta = g \text{ on } \partial E.$$

Thanks to this fact, the dimension of $V_{k,\delta}^{\text{old}}(E)$ is

$$\dim(V_{k,\delta}^{\text{old}}(E)) = n_v k + \frac{k(k-1)}{2}, \tag{2.3}$$

where n_v is the number of vertices of E and the last term corresponds to the dimension of polynomials in two dimensions of degree less or equal than $k-2$. The following set of degrees of freedom is chosen in $V_{k,\delta}^{\text{old}}(E)$:

(D1) the value of $v_\delta \in V_{k,\delta}^{\text{old}}(E)$ at the vertices of E;

(D2) the value of $v_\delta \in V_{k,\delta}^{\text{old}}(E)$ at the $k-1$ internal points of the $(k+1)$-point Gauss-Lobatto quadrature rule on e, for each edge e of E;

(D3) if $k \geq 2$, the scaled moments are used:

$$\frac{1}{|E|} \int_E v_\delta m, \quad \forall m \in \mathcal{M}_{k-2}(E),$$

where $n_{k-2} = \frac{k(k-1)}{2}$ is the number of functions in $\mathcal{M}_{k-2}(E)$ and $|E|$ is the area of E.

In literature [2, 8], it's possible to find a different set of DOFs, substituting (D2) with:

(D2') for $k \geq 2$, the moments $\int_e v_\delta p_{k-2}$, for $p_{k-2} \in \mathbb{P}_{k-2}(e)$ and any edges e of E. It's feasible to use scaled monomials instead on "standard" polynomials.

The number of DOFs is:

$$\#\text{DOFs} = n_v + n_v(k-1) + \frac{k(k-1)}{2} \equiv \dim\left(V_{k,\delta}^{\text{old}}(E)\right).$$

It has been demonstrated in [5] that the chosen set of degrees of freedom is unisolvent for $V_{k,\delta}^{\text{old}}(E)$.
Let's define the operator $\text{dof}_i : V_{k,\delta}^{\text{old}}(E) \to \mathbb{R}$ such that, for $v_\delta \in V_{k,\delta}^{\text{old}}(E)$,

$$\text{dof}_i\left(v_\delta\right) := i \text{ th-degree of freedom of } v_\delta, \quad i = 1, \ldots, \dim(V_{k,\delta}^{\text{old}}(E)). \tag{2.4}$$

The basis functions $\varphi_i \in V_{k,\delta}^{\text{old}}(E)$ are defined as the Lagrange basis functions:

$$\text{dof}_i\left(\varphi_j\right) = \delta_{ij}, \quad i,j = 1, \ldots, \dim(V_{k,\delta}^{\text{old}}(E)), \tag{2.5}$$

$$v_\delta = \sum_{i=1}^{\dim(V_{k,\delta}^{\text{old}}(E))} \text{dof}_i\left(v_\delta\right)\varphi_i, \quad \text{for all } v_\delta \in V_{k,\delta}^{\text{old}}(E).$$

It may be interesting to note that, in case $k = 1$, there are no internal degrees of freedom and the local VEM space coincides with the local FEM space, in case the mesh $\tau_{\delta,i}$ contains only triangles.

Articles such as [7, 19] introduce a new VEM space right from the beginning of the VEM discussion. This space involves the definition of a projection operator that will be crucial in the implementation and the reason for this change will become clearer later.

$$\begin{aligned} V_{k,\delta}(E) = \big\{ & v_\delta \in \mathrm{H}^1(E) : v_{\delta|\partial E} \in C^0(\partial E), \quad v_{\delta|e} \in \mathbb{P}_k(e), \forall e \subset \partial E \\ & \Delta v_\delta \in \mathbb{P}_k(E), \quad \int_E v_\delta p = \int_E \Pi_{E,k}^{\nabla}(v_\delta) p, \quad \forall p \in \mathbb{P}_k(E) \setminus \mathbb{P}_{k-2}(E) \Big\}, \end{aligned} \tag{2.6}$$

where the space $\mathbb{P}_k(E) \setminus \mathbb{P}_{k-2}(E)$ is the space of polynomials on E of degrees k or $k-1$, and

$$\Pi_{E,k}^{\nabla} : V_{k,\delta}(E) \longrightarrow \mathbb{P}_k(E)$$

is the $H^1(E)$-orthogonal operator defined as, for all $v_\delta \in V_{k,\delta}(E)$,

$$\begin{aligned} & \int_E \nabla p_k \cdot \left(\nabla v_\delta - \nabla \Pi_{E,k}^{\nabla}(v_\delta)\right) = 0 \quad \forall p_k \in \mathbb{P}_k(E), \\ & \begin{cases} \int_E \Pi_{E,k}^{\nabla}(v_\delta) = \int_E v_\delta & k > 1, \\ \int_{\partial E} \Pi_{E,k}^{\nabla}(v_\delta) = \int_{\partial E} v_\delta & k = 1. \end{cases} \end{aligned} \tag{2.7}$$

Let's notice that the conditions included in the curly bracket are crucial for the definition. Without these conditions, the projection operator would only be defined up to an arbitrary constant.

Remark 4. *It's very important to observe that the choice of the projection operator may vary, independently on the used local virtual element space. Actually, curly brackets equalities can be resumed with*

$$\mathcal{R}\Big(\Pi^{\nabla}_{E,k}(v_\delta) - v_\delta\Big) = 0,$$

where $\mathcal{R}$ represents any projection operator onto the space $\mathbb{P}_0(E)$, as stated in [4, 20]. In the literature one can find various choices for the operator $\mathcal{R}$:

- *the one defined in* (2.7) *has been implemented in [2];*
- *in [6, 10, 11, 12] the condition for $k = 1$ is substituted with :*

$$\sum_{i=1}^{n_v} \left(\Pi^{\nabla}_{E,k}(v_\delta)\right)(\mathcal{V}_i) = \sum_{i=1}^{n_v} v_\delta\left(\mathcal{V}_i\right), \tag{2.8}$$

  where the vertices of E are denoted by $\mathcal{V}_i$;

- *in [7, 8] a single condition is used, regarding only integration on the boundary of E:*

$$\int_{\partial E} \Pi^{\nabla}_{E,k}(v_\delta) = \int_{\partial E} v_\delta$$

  Basically, this is the second one in (2.7) *extended for all $k \geq 1$.*

Proposition 1. *Here's some properties:*

P1 - *$V_{k,\delta}(E)$ contains $\mathbb{P}_k(E)$;*

P2 - *the same degrees of freedom used for the previous space can be employed preserving unisolvence, because $\dim(V_{k,\delta}(E)) = \dim(V^{old}_{k,\delta}(E))$;*

P3 - *the projection operator is easily computable using the degrees of freedom (D1)-(D2)-(D3). Consequently, the basis functions φ_i defined in* (2.5) *are the same;*

P4 - *if $v^1_\delta \in V_{k,\delta}(E)$ and $v^2_\delta \in V^{old}_{k,\delta}(E)$ share the same DOFs $\implies \Pi^{\nabla}_{E,k}(v^1_\delta) = \Pi^{\nabla}_{E,k}(v^2_\delta)$;*

Proof. A very useful property of the projection operator follows:

$$\Pi^{\nabla}_{E,k}(p_k) = p_k \text{ for all } p_k \in \mathbb{P}_k(E), \tag{2.9}$$

because p_k and $\Pi^{\nabla}_{E,k}(p_k)$ has the same gradient from the first equation. Clearly, $(P1)$ is true.
As in [2], for $k \geq 1$, let's define this new space:

$$\tilde{V}_{k,\delta}(E) := \{\, v_\delta \in \mathrm{H}^1(E) : v_{\delta|\partial E} \in C^0(\partial E), v_{\delta|e} \in \mathbb{P}_k(e), \forall e \subset \partial E, \Delta v_\delta \in \mathbb{P}_k(E) \,\},$$

where ∂E indicates the boundary of E and e is an edge on that boundary. Recalling the proof in (2.3), its dimension is:

$$\dim(\tilde{V}_{k,\delta}(E)) = n_v k + \frac{(k+2)(k+1)}{2}.$$

Now, the number of scaled monomials that can be used as basis for $\mathbb{P}_k(E) \setminus \mathbb{P}_{k-2}(E)$, in the definition of the new VEM space $V_{k,\delta}(E)$, is $2k+1$. Not knowing if these additional conditions are indipendent, follows that:

$$\dim(V_{k,\delta}(E)) \geq \dim(\tilde{V}_{k,\delta}(E)) - (2k+1) = n_v k + \frac{k(k-1)}{2}. \tag{2.10}$$

Consider a function $w_\delta \in V_{k,\delta}(E)$ that vanishes on ∂E and has zero moments up to order $k-2$ is identically zero. From the definition (2.7) using integration by parts, for all $p_k \in \mathbb{P}_k$, observe that:

$$\int_E \nabla p_k \cdot \left(\nabla w_\delta - \nabla \Pi^\nabla_{E,k}(w_\delta)\right) = 0 \implies -\int_E w_\delta \Delta p_k + \int_{\partial E} w_\delta \frac{\partial p_k}{\partial n} = \int_E \nabla \Pi^\nabla_{E,k}(w_\delta) \cdot \nabla p_k.$$

Since $\Delta p_k \in \mathbb{P}_{k-2}$ and thanks to the property about moments of w_δ, the first integral on the left side of the equality is null; the second one is equal to zero because $w_\delta \equiv 0$ on ∂E. Then $\Pi^\nabla_{E,k}(w_\delta)$ is a constant and thanks to the additional conditions in (2.7), this is zero. This implies that all the moments of $\Pi^\nabla_{E,k}(w_\delta)$ are zero. Since $w_\delta \in V_{k,\delta}(E)$, all the moments of order $k-1$ and k are also zero. Thanks to Proposition 1 in [2], it's possible to consider as DOFs in $\tilde{V}_{k,\delta}(E)$ the traces on ∂E and the moments up to order k: it implies that w_δ is zero.
This fact, together with (2.10), proves

$$\dim(V_{k,\delta}(E)) = \dim(V^{\text{old}}_{k,\delta}(E)),$$

and that in the new space the (D1)-(D2)-(D3) set of DOFs are unisolvent.

Let's see the proof of (P3) following [6], using the equivalent condition (2.8). The first equation in (2.7) can be considered only for scaled monomials because they generate a basis for $\mathbb{P}_k(E)$. Same idea for $\Pi^\nabla_{E,k}(v_\delta)$. Recalling that $n_k = \dim(\mathbb{P}_k(E))$,

$$\Pi^\nabla_{E,k}(v_\delta) = \sum_{\beta=1}^{n_k} s^\beta m_\beta.$$

The orthogonality condition becomes:

$$\sum_{\beta=1}^{n_k} s^\beta \left(\nabla m_i, \nabla m_\beta\right)_E = \left(\nabla m_i, \nabla v_\delta\right)_E, \quad i = 1, \dots, n_k. \tag{2.11}$$

This corresponds to a linear system of n_k equation in n_k unknowns. The second and third equations in (2.7) solve the indeterminacy when $i = 1$: in this case $m_i \equiv 1$ and the equation (2.11) becomes $0 = 0$. Basically, the following equation is being added to the system:

$$\begin{cases} \displaystyle\sum_{\beta=1}^{n_k} s^\beta \int_E m_\beta = \int_E v_\delta & k > 1, \\ \displaystyle\sum_{i=1}^{n_v} \sum_{\beta=1}^{n_k} s^\beta m_\beta(\mathcal{V}_i) = \sum_{i=1}^{n_v} v_\delta(\mathcal{V}_i) & k = 1, \end{cases} \tag{2.12}$$

The linear system can be written using matrices:

$$\mathbf{G}s = b$$

where:

$$\mathbf{G} := \begin{bmatrix} \mathrm{P}_0(m_1) & \mathrm{P}_0(m_2) & \cdots & \mathrm{P}_0(m_{n_k}) \\ 0 & (\nabla m_2, \nabla m_2)_E & \cdots & (\nabla m_2, \nabla m_{n_k})_E \\ \vdots & \vdots & \ddots & \vdots \\ 0 & (\nabla m_{n_k}, \nabla m_2)_E & \cdots & (\nabla m_{n_k}, \nabla m_{n_k})_E \end{bmatrix}$$

and

$$b := \begin{bmatrix} \mathrm{P}_0(v_\delta) \\ (\nabla m_2, \nabla v_h)_E \\ \vdots \\ (\nabla m_{n_k}, \nabla v_\delta)_E \end{bmatrix} \qquad s := \begin{bmatrix} s^1 \\ \vdots \\ s^{n_k} \end{bmatrix}.$$

The operator P_0 refers to this double possibilities (2.12). In order to compute $\Pi^\nabla_{E,k}(v_\delta)$ using only DOFs, it must be shown that b is computable from these. By definition, $\mathrm{P}_0(v_\delta)$ has this property, while, for the other components of b:

$$(\nabla m_i, \nabla v_\delta)_E = -\int_E \Delta m_i v_\delta + \int_{\partial E} \frac{\partial m_i}{\partial n} v_\delta$$

obtained using integration by parts. Using the fact that $\Delta m_i \in \mathbb{P}_{k-2}(E)$, it can be expressed as a linear combination of the n_{k-2} scaled monomials:

$$\Delta m_i = \sum_{\beta=1}^{n_{k-2}} d_i^\beta m_\beta$$

and

$$\int_E \Delta m_i v_\delta = \sum_{\beta=1}^{n_{k-2}} d_i^\beta \int_E m_\beta v_\delta = -|E| \sum_{\beta=1}^{n_{k-2}} d_i^\beta \, \mathrm{dof}_{(kn_v+\beta)}(v_\delta).$$

The second terms involves an integration of a polynomial of degree $(k-1)+k = 2k-1$ on each edge of ∂E: thanks to the choice of Gauss–Lobatto quadrature points the integration will be exact. This is straightforward since the values of v_δ at these locations directly represent its degrees of freedom. For a complete discussion, including the calculation of $\Pi^\nabla_{E,k}(\varphi_i)$, refer to [6].

Finally, (P4) is implied by the previous property.

□

Remark 5. *Note that* (2.7) *defines the operator* $\Pi^\nabla_{E,k}(v_\delta)$ *on the whole space* $H^1(E)$*, and not only on* $V_{k,\delta}(E)$*, but of course it is not computable in general (see [2]).*

A comparison with FEM in terms of the number of DOFs for a given degree $k \geq 1$, shows that the boundary DOFs are exactly as expected on both triangles and quadrilaterals, since they must guarantee global continuity. In VEM case, the number of internal DOFs is at least the dimension of $\mathbb{P}_{k-2}$ for any polygon. In contrast, for FEM, this number is equal to the dimension of $\mathbb{P}_{k-3}$ on triangles and $\mathbb{Q}_{k-3}$ on quadrilaterals, where $\mathbb{Q}_r$ denotes polynomials of degree r separately

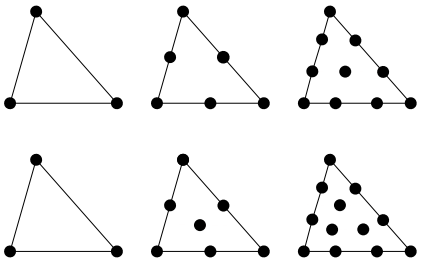

Figure 2.1: DOFs on triangles: from left to right, $k = 1, 2, 3$ for FEM (first row) and VEM (second row).

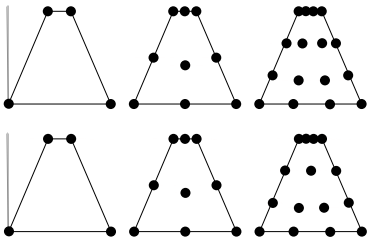

Figure 2.2: DOFs on quads: from left to right, $k = 1, 2, 3$ for FEM (first row) and VEM (second row).

in each variable. As can be seen in Figure 2.1 and 2.2, on triangles a VEM uses $k-1$ more DOFs than a FEM, while on quadrilaterals, a FEM uses $\frac{(k-1)(k-2)}{2}$ more degrees of freedom than a VEM.

The global virtual element space $V_{k,\delta}(F_i)$ on F_i is:

$$V_{k,\delta}\left(F_i\right) = \left\{v_\delta \in H_0^1(F_i) : v_\delta|_E \in V_{k,\delta}(E) \text{ for all } E \in \tau_{\delta,i}\right\},$$

and the global degrees of freedom for $v_\delta \in V_{k,\delta}\left(F_i\right)$ are:

- the value of v_δ at the internal vertices of the decomposition;
- the value of v_δ at the $k-1$ internal points of the $(k+1)$ points of Gauss-Lobatto quadrature rule on each internal edge e;
- the scaled moments up to order $k-2$ in each polygon E.

The other operator that is needed is defined as follows: basically is the L^2-projection. For every function $v_\delta \in V_{k,\delta}(E)$ and $k \geq 0$, the polynomial $\Pi^0_{E,k}(v_\delta) \in \mathbb{P}_k(E)$ is defined by an orthogonality condition:

$$\left(\Pi^0_{E,k}(v_\delta), p\right)_E = \left(v_\delta, p\right)_E \qquad \forall p \in \mathbb{P}_k(E), \quad \forall v_\delta \in V_{k,\delta}(E). \tag{2.13}$$

Originally, using the old space $V^{\text{old}}_{k,\delta}(E)$, the operator is introduced in [6] as:

$$\begin{aligned}
&\left(\Pi^0_{E,k}(v_\delta), p\right)_E = (v_\delta, p)_E \qquad \forall p \in \mathbb{P}_{k-2}(E), \quad \forall v_\delta \in V^{\text{old}}_{k,\delta}(E).\\
&\left(\Pi^0_{E,k}(v_\delta), p\right)_E = \left(\Pi^\nabla_{E,k}(v_\delta), p\right)_E \qquad \forall p \in \mathbb{P}_k(E) \setminus \mathbb{P}_{k-2}(E), \quad \forall v_\delta \in V^{\text{old}}_{k,\delta}(E).
\end{aligned} \tag{2.14}$$

The use of $V_{k,\delta}(E)$ makes it possible to state that (2.13) and (2.14) are the same on $V_{k,\delta}(E)$. Moreover, the definition of $\Pi^0_{E,k}$ can be extented for every function in $L^2(E)$.

2.2 VEM in the DFN context

The flexibility of the VEM approach enables modifications to a given triangulation, created disregarding trace positions, splitting the triangles along traces: polygons can vary in the number of vertices. The initial one is called *base mesh* and the new polygonal mesh, locally conforming to the traces of the fractures is called *VEM mesh*. Later on, a detailed explanation will be provided on how to obtain such a mesh.

A quick look at the first term of the equation (1.1) reveals that it is necessary to compute a local stiffness matrix, associated with the bilinear form defined on each $E \subset F_i$:

$$a^E(u,v) = K_i(\nabla u, \nabla v)_E \quad \forall u, v \in V_{k,\delta}(E). \tag{2.15}$$

Remember that the value K_i is constant over the entire fracture F_i.
Unlike in FEM, it is not necessary to have the explicit form of the basis functions φ_i, which is why the method is referred to as "virtual". One of the keys of the VEM method is the use of the previous defined projection operators on E, respectively (2.7) and (2.13), essential for the introduction of discrete linear forms. The effect of choosing the K_i values as constants influences the choice of projections: in the case of non-constant coefficients or elliptic problems with additional terms, different operators must be selected [7].
The first discrete symmetric bilinear form

$$a^E_\delta : V_{k,\delta}(E) \times V_{k,\delta}(E) \longrightarrow \mathbb{R}$$

on the element E needs the definition of $S^E_\delta : V_{k,\delta}(E) \times V_{k,\delta}(E) \longrightarrow \mathbb{R}$, a symmetric positive definite bilinear form such that :

$$\exists C_0, C_1 > 0 \text{ independent of } E: \quad C_0 a^E(v_\delta, v_\delta) \leq S^E_\delta(v_\delta, v_\delta) \leq C_1 a^E(v_\delta, v_\delta), \tag{2.16}$$

for all $v_\delta \in \ker\left(\Pi^\nabla_{E,k}\right)$. This form scales like $a^E(\cdot,\cdot)$ on the kernel of $\Pi^\nabla_{E,k}$. The choice of the bilinear form $a^E_\delta(\cdot,\cdot)$ can vary:

- in this thesis, the approach presented in [7, 8] is adopted:

$$\begin{aligned} a^E_\delta(u_\delta, v_\delta) = &\left(K_i \Pi^0_{E,k-1}(\nabla u_\delta), \Pi^0_{E,k-1}(\nabla v_\delta)\right)_E \\ &+ S^E_\delta\left(u_\delta - \Pi^\nabla_{E,k}(u_\delta), v_\delta - \Pi^\nabla_{E,k}(v_\delta)\right), \quad \forall u_\delta, v_\delta \in V_{k,\delta}(E); \end{aligned} \tag{2.17}$$

- in [4, 5, 6, 8, 10, 11, 12] the following form is used:

$$\begin{aligned} a^E_\delta(u_\delta, v_\delta) = &\, a^E\left(\Pi^\nabla_{E,k}(u_\delta), \Pi^\nabla_{E,k}(v_\delta)\right) \\ &+ S^E_\delta\left(u_\delta - \Pi^\nabla_{E,k}(u_\delta), v_\delta - \Pi^\nabla_{E,k}(v_\delta)\right), \quad \forall u_\delta, v_\delta \in V_{k,\delta}(E), \end{aligned}$$

Actually, it can be seen that for $k = 1$ both forms coincides and this doesn't happen for $k \geq 2$. As said in [7], heavy losses has been noticed for $k \geq 3$ using the second bilinear form. This fact led to the choice adopted.

In order to obtain a convergence theorem for the discrete version of a general variational problem

$$\text{find } u \in V \text{ such that } a(u,v) = (f,v)_V \quad \forall v \in V$$

(see Theorem 3.1 in [5]), this new bilinear form (2.17) must have these two properties with respect to $a^E(\cdot,\cdot)$ defined in (2.15):

- *k-Consistency*: $\forall p \in \mathbb{P}_k(E)$ and $\forall v_\delta \in V_{k,\delta}(E)$,
$$a_\delta^E(p, v_\delta) = a^E(p, v_\delta). \tag{2.18}$$
- *Stability*: $\exists \alpha_*, \alpha^* > 0$ constants independent of δ and of E, such that
$$\forall v_\delta \in V_{k,\delta}(E), \quad \alpha_* a^E(v_\delta, v_\delta) \leq a_\delta^E(v_\delta, v_\delta) \leq \alpha^* a^E(v_\delta, v_\delta).$$

Proposition 2. *Assume K_i is constant over the entire fracture F_i. Both properties of k-consistency and stability are satisfied if the* (2.17) *bilinear form is considered.*

Proof. For all $p \in \mathbb{P}_k(E)$, (2.9) implies $S_\delta^E\left(p - \Pi_{E,k}^\nabla(p), v_\delta - \Pi_{E,k}^\nabla(v_\delta)\right) = 0$ and this ensures the *k-Consistency* because

$$\begin{aligned} a_\delta^E(p, v_\delta) &\overset{(2.17)}{=} \left(K_i \Pi_{E,k-1}^0(\nabla p), \Pi_{E,k-1}^0(\nabla v_\delta)\right)_E \overset{(2.13)}{=} \left(K_i \nabla p, \Pi_{E,k-1}^0(\nabla v_\delta)\right)_E \\ &\overset{(2.13)}{=} \left(K_i \nabla p, \nabla v_\delta\right)_E \overset{(2.15)}{=} a^E(p, v_\delta). \end{aligned}$$

Some properties of $\Pi_{E,k}^\nabla$ are used in order to proof stability. For all $v_\delta \in V_{k,\delta}(E)$

$$\begin{aligned} \left(\nabla[v_\delta - \Pi_{E,k}^\nabla(v_\delta)], \nabla[v_\delta - \Pi_{E,k}^\nabla(v_\delta)]\right)_E &\overset{(2.7)}{=} \left(\nabla[v_\delta - \Pi_{E,k}^\nabla(v_\delta)], \nabla v_\delta\right)_E \\ &\leq |v_\delta - \Pi_{E,k}^\nabla(v - \delta)|_{1,E} |v_\delta|_{1,E}, \end{aligned}$$

which gives

$$|v_\delta - \Pi_{E,k}^\nabla(v_\delta)|_{1,E} \leq |v_\delta|_{1,E}. \tag{2.19}$$

The second property is valid for all $u_\delta, v_\delta \in V_{k,\delta}(E)$ such that $\Pi_{E,k}^\nabla(u_\delta) = \Pi_{E,k}^\nabla(v_\delta) = 0$.

$$S_\delta^E(u_\delta, v_\delta) \leq (S_\delta^E(u_\delta, u_\delta))^{\frac{1}{2}} (S_\delta^E(v_\delta, v_\delta))^{\frac{1}{2}} \overset{(2.16)}{\leq} C_1 (a^E(u_\delta, u_\delta))^{\frac{1}{2}} (a^E(v_\delta, v_\delta))^{\frac{1}{2}}. \tag{2.20}$$

Now, for all $v_\delta \in V_{k,\delta}(E)$, since

$$\Pi_{E,k}^\nabla(v_\delta - \Pi_{E,k}^\nabla(v_\delta)) \overset{(2.9)}{=} \Pi_{E,k}^\nabla(v_\delta) - \Pi_{E,k}^\nabla(v_\delta) = 0,$$

(2.20) can be used below:

$$\begin{aligned} S_\delta^E\left(v_\delta - \Pi_{E,k}^\nabla(v_\delta), v_\delta - \Pi_{E,k}^\nabla(v_\delta)\right) &\overset{(2.20)}{\leq} C_1 K_i |v_\delta - \Pi_{E,k}^\nabla(v_\delta)|_{1,E}^2 \\ &\overset{(2.19)}{\leq} C_1 K_i |v_\delta|_{1,E}^2 \overset{K_i \text{ is constant}}{=} \alpha^* a^E(v_\delta, v_\delta). \end{aligned}$$

Finally, using the proof of Lemma 5.2 in [7],

$$a_\delta^E(v_\delta, v_\delta) \leq (1 + C_1)a^E(v_\delta, v_\delta)$$

so the right inequality of the stability property is obtained. Following the proof of Lemma 5.6 in [7], by definition of projection

$$\|\nabla v_\delta - \Pi^0_{E,k-1}(\nabla v_\delta)\|_E \leq \|\nabla v_\delta - \Pi^\nabla_{E,k-1}(\nabla v_\delta)\|_E.$$

Then, for all $v_\delta \in V_{k,\delta}(E)$

$$a_\delta^E(v_\delta, v_\delta) \geq \alpha_* \|\Pi^0_{E,k-1}(\nabla v_\delta)\|_E^2 + \|(I - \Pi^0_{E,k-1})\nabla v_\delta\|_E^2 \geq \alpha_* |v_\delta|_1^2$$

□

The choice of the bilinear form S_δ^E can vary: in this thesis, we will follow the approach presented in [5, 6], but it is advisable to consult [4] to better understand all the options. All these choices have in common is that $S_\delta^E(\cdot,\cdot)$ must scale like $a^E(\cdot,\cdot)$ on $\ker(\Pi^\nabla_{E,k})$.

Assumption 1. *$\exists \sigma > 0$ constant independent of δ such that, $\forall E \in \tau_{\delta,i}$ and $\forall i = 1, \ldots, N$, the distance between any two vertices of E is larger then or equal to σh_E, where h_E is the diameter of E.*

Thanks to this assumption, it's possible to choose:

$$S_\delta^E\Big(\varphi_i - \Pi^\nabla_{E,k}(\varphi_i), \varphi_j - \Pi^\nabla_{E,k}(\varphi_j)\Big) = \sum_{r=1}^{\#V_{k,\delta}(E)} \mathrm{dof}_r(\varphi_i - \Pi^\nabla_{E,k}(\varphi_i))\,\mathrm{dof}_r(\varphi_j - \Pi^\nabla_{E,k}(\varphi_j))$$

for all canonical basis function in $\{\varphi_i\}_{i=1}^{\#V_{k,\delta}(E)}$. With this choice, (2.16) is verified (see [5]).

The next step in the DFN context is to define the global discrete bilinear form. Here's some definitions:

$$V_{k,\delta} = \prod_{i=1}^N V_{k,\delta}(F_i), \qquad a_\delta : V_{k,\delta} \times V_{k,\delta} \longrightarrow \mathbb{R},$$

$$a_\delta(u_\delta, v_\delta) = \sum_{i=1}^N \sum_{E \in \tau_{i,\delta}} a_\delta^E(u_{\delta|E}, v_{\delta|E}), \quad \forall u_\delta, v_\delta \in V_{k,\delta}, \tag{2.21}$$

where the symbol used indicates that the restriction of the function to E is being considered.
k-Consistency and *stability* of the local discrete symmetric bilinear form are useful to state that $a_\delta(\cdot,\cdot)$ is equivalent to $a(\cdot,\cdot)$ defined in (1.11), i.e, $\exists \alpha_*, \alpha^* > 0$ independent of δ and of E such that, $\forall v_\delta \in V_{k,\delta}$,

$$\alpha_* a\left(v_\delta, v_\delta\right) \leq a_\delta\left(v_\delta, v_\delta\right) \leq \alpha^* a\left(v_\delta, v_\delta\right). \tag{2.22}$$

It's easy to check that:

$$\begin{aligned} a_\delta\left(v_\delta, v_\delta\right) &= \sum_{i=1}^N \sum_{E \in \tau_{i,\delta}} a_\delta^E(v_{\delta|E}, v_{\delta|E}) \leq \sum_{i=1}^N \sum_{E \in \tau_{i,\delta}} \alpha^* a^E(v_{\delta|E}, v_{\delta|E}) \\ &= \alpha^* a\left(v_\delta, v_\delta\right). \end{aligned}$$

The proof is the same for the reverse inequality.

Concerning the right hand side of (1.1), it's possible to have different discretizations. This choice is influenced also by the local virtual element space used between $V_{k,\delta}^{\text{old}}(E)$ and $V_{k,\delta}(E)$:

- $V_{k,\delta}^{\text{old}}(E)$: in this case, [6, 10] uses

$$(f_i, v_\delta)_\delta := \sum_{E \in \tau_{i,\delta}} \int_E f_E \Pi^0_{E,k}(v_\delta) \qquad \forall v_\delta \in V_{k,\delta}^{\text{old}}(F_i), \quad \forall i = 1, \dots, N,$$

  where the restriction of f to F_i is f_i, the restriction of f to E is f_E and $V_{k,\delta}^{\text{old}}(F_i)$ is the counterpart of $V_{k,\delta}(F_i)$ using $V_{k,\delta}^{\text{old}}(E)$ on each $E \subset F_i$.
  Alternatively, [2, 5, 8] uses, for $k \geq 2$:

$$(f_i, v_\delta)_\delta := \sum_{E \in \tau_{i,\delta}} \int_E v_\delta \Pi^0_{E,k-2}(f_E) \qquad \forall v_\delta \in V_{k,\delta}^{\text{old}}(F_i), \quad \forall i = 1, \dots, N. \tag{2.23}$$

- $V_{k,\delta}(E)$: this case is the most interesting, since it's the one implemented in the following chapters.

$$(f_i, v_\delta)_\delta := \sum_{E \in \tau_{i,\delta}} \int_E f_E \Pi^0_{E,k-1}(v_\delta) \qquad \forall v_\delta \in V_{k,\delta}(F_i), \quad \forall i = 1, \dots, N, \tag{2.24}$$

  like in [7, 8].

As in (2.21), the global discrete form for the right hand side is:

$$(f, v_\delta)_\delta := \sum_{i=1}^{N} \sum_{E \in \tau_{i,\delta}} \int_E f_E \Pi^0_{E,k-1}(v_\delta) \qquad \forall v_\delta \in V_{k,\delta}. \tag{2.25}$$

The notation is the same, but it will be clear from the context which one is used. Note that the application of the L^2-projector to v_δ or f_E in the previous definition is equivalent. For example,

$$\left(f_E, \Pi^0_{E,k-1}(v_\delta)\right)_E \overset{(2.13)}{=} \left(\Pi^0_{E,k-1}(f_E), \Pi^0_{E,k-1}(v_\delta)\right)_E \overset{(2.13)}{=} \left(\Pi^0_{E,k-1}(f_E), v_\delta\right)_E.$$

Remark 6. *Following [8], the use of $V_{k,\delta}(E)$ instead of $V_{k,\delta}^{old}(E)$ allows to compute the L^2-projection onto $\mathbb{P}_k(E)$. This can be used to compute an approximation of the right-hand side as* (2.24) *that is simpler than the original one described in* (2.23).

Chapter 3

Mortar element method and its application

The mortar element method, first introduced in [13, 14], is a domain decomposition technique that takes advantage of the division in subdomains of the principal domain. The main reason for its use is to be able to choose the most suitable discretization method for the local behavior of the solution of the equation being approximated.
Compared to other domain decomposition methods, one of the key benefits of the mortar element method is its flexibility in handling different types of non-conformities. Even though the meshes on the subdomains do not align, Lagrange multipliers are used to ensure the equality of the solution across the interface, preserving its accuracy. Mortar discretizations are well-suited for solving with iterative domain decomposition methods like FETI and balancing domain decomposition [21, 23, 24, 26].
As already mentioned in the initial introduction, the mortar method is applied after the VEM approach: specifically, the coupling of these two methods is achieved by using a mortar interpretation on the finite-dimensional approximation of V obtained with VEM [10].
Section 3.1 will describe and analyze the mortar method in general. Section 3.2 will apply it to the DNF problem addressed with VEM. Section 3.3 provides the well-posedness analysis of the discrete problem obtained in the previous section and Section 3.4 gives an a priori error estimates.

3.1 Description of the mortar element method

This section will follow the method description found in [29]. It's important to note that the notations used in this section are self-referential and will be correlated with those employed in the preceding chapters only in the following sections.
Let's take Ω be a bounded connected domain in $\mathbb{R}^2$ decomposed into K non-overlapping polygonal open subdomains $\Omega_k \geq 1$ such that

$$\overline{\Omega} = \cup_{k=1}^{K} \overline{\Omega}_k \quad \text{and} \quad \Omega_k \cap \Omega_l = \emptyset, \quad 1 \leq k \neq l \leq K.$$

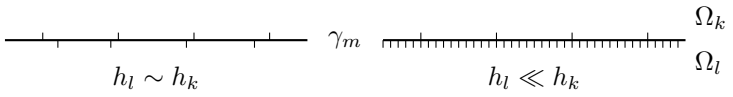

Figure 3.1: Example of different discretizations on two subdomains Ω_k and Ω_l that shares an intersection γ_m.

In general, the decomposition is said to be geometrically conforming if the intersection of two different subdomains Ω_k is either empty or a vertex or a whole edge or a whole face of both of them. Neither this restriction nor any others are imposed on the decomposition a priori. On each subdomain is defined a discretization τ_{k,h_k} with h_k bound for the mesh-size. Since the subdomains will be identified on the fractures (see the Section 3.2), as in the case of VEM, a key aspect of defining this method is the determination of their intersections. The interfaces are denoted by γ_m, $1 \leq m \leq M$, such that there exist $l, k \in \{1, \ldots, K\}$:

$$\overline{\gamma}_m = \partial\Omega_l \cap \partial\Omega_k.$$

In general, the two discretizations τ_{k,h_k} and τ_{l,h_l} do not coincide, as shown in Figure 3.1. A $(d-1)$-dimensional decomposition discretization on γ_m, called S_{m,h_m}, can be defined using one of the two previous ones; its elements are boundary edges. The subdomain from which the decomposition is inherited is called the non-mortar $\Omega_{n(m)}$, while the other is referred to as the mortar $\Omega_{\overline{n}(m)}$, where it's introduced the notation $n(m), \overline{n}(m)$ to distinguish between the two subdomains. This is the real strength of the mortar method: it allows for the independent discretization of the two subdomains. It is also possible to introduce a new independent decomposition on each interface γ_m. which is inherited neither from $\tau_{n(m),h_{n(m)}}$ or $\tau_{\overline{n}(m),h_{\overline{n}(m)}}$ [29].

X_{h_k,n_k} is the finite dimensional space on Ω_k associated with τ_{k,h_k}, which functions satisfies homogeneous Dirichlet boundary conditions on $\partial\Omega \cap \partial\Omega_k$. It must contains $\mathbb{P}_{n_k}(\Omega_k)$: in [29], X_{h_k,n_k} is the canonical finite element space, while [15] examines the application of this method to spectral elements and a coupling between spectral and finite elements method.

To derive the mortar approximation u_h as a solution to a discrete variational problem, two principal approaches have been developed. The first approach [13, 14] results in a positive definite nonconforming variational problem. This method is defined on a subspace V_h of the product space of X_{h_k,n_k}, where the elements satisfy weak continuity conditions at the interfaces. This constrained space V_h is specified by the following definition:

$$\begin{aligned} V_h := \{v \in L^2(\Omega) | \quad & v_{|\Omega_k} \in X_{h_k,n_k}, \quad 1 \leq k \leq K, \\ & \int_{\gamma_m} [\![v]\!] \mu d\sigma = 0, \quad \forall \mu \in M_{h_m}(\gamma_m), \quad 1 \leq m \leq M\}, \end{aligned} \tag{3.1}$$

where the test space is given by

$$\begin{aligned} M_{h_m}(\gamma_m) := \{\mu \in L^2(\gamma_m) | \quad & \mu = w_{|\gamma_m}, w \in X_{h_{n(m)},n_{n(m)}}, \\ & \mu_{|e} \in \mathbb{P}_{n_m-1}(e), \text{ if } e \in S_{m,h_m} \text{ contains an endpoint of } \gamma_m\}, \end{aligned} \tag{3.2}$$

and $n_m := n_{n(m)}$.

Given a uniform elliptic bilinear form $a(\cdot,\cdot)$, defined in [29], and $f \in L^2(\Omega)$, the nonconforming formulation of the mortar method is defined on the constrained space:

$$\text{find } u_h \in V_h \text{ such that } a(u_h, v_h) = (f, v_h)_\Omega, \quad \forall v_h \in V_h. \tag{3.3}$$

Well-posedness and a priori estimates are detailed in [29]. Replacing V_h in the variational formulation gives rise to a saddle-point problem, which is the core of the second approach [9, 28]. It's defined

$$X_h = \{\, v \in L^2(\Omega) \mid \quad v_{|\Omega_k} \in X_{h_k,n_k}, \quad 1 \le k \le K \,\}, \tag{3.4}$$

and

$$M_h = \prod_{m=1}^{M} M_{h_m}(\gamma_m), \quad \forall \gamma_m. \tag{3.5}$$

The goal is to find $(u_h, v_h) \in (X_h, M_h)$ such that

$$\begin{cases} a(u_h, v) + b(v, \lambda_h) = (f, v)_\Omega, & v \in X_h, \\ b(u_h, \mu) = 0, & \mu \in M_h. \end{cases} \tag{3.6}$$

where the bilinear form $b(\cdot,\cdot)$ is given by the duality pairing on the interfaces

$$b(v,\mu) = \sum_{m=1}^{M} \langle [\![v]\!], \mu \rangle_{\pm\frac{1}{2},\gamma_m}, \quad v \in \prod_{k=1}^{K} H^1(\Omega_k), \quad \mu \in \prod_{m=1}^{M} \left(H^{\frac{1}{2}}(\gamma_m)\right)'$$

and $[\![v]\!] = v_{|\Omega_{n(m)}} - v_{|\Omega_{\overline{n}(m)}}$.
Thus, the two approaches give rise to two problems that have the same solution u_h, while the discrete Lagrange multiplier λ_h approximates the flux. As in the general saddle-point approach, the essential point in order to obtain well-posedness is to establish an adequate inf-sup condition, with constant independent of the mesh-size. See [9, 28] for a detailed analysis of this issue.

Before defining the basis for the discrete spaces of Lagrange multipliers that will be used in the implementation section following the methodology of [10], it is necessary to introduce new multiplier spaces. Firstly,

$$W_{h_m}(\gamma_m) = \{\, \mu \in C^0(\gamma_m) \mid \quad \mu = w_{|\gamma_m}, w \in X_{h_{n(m)},n_{n(m)}} \,\} \tag{3.7}$$

and

$$W_{0,h_m}(\gamma_m) = W_{h_m}(\gamma_m) \cap H_0^1(\gamma_m) \tag{3.8}$$

are presented. A subspace called $M_{h_m}(\gamma_m)$ of $L^2(\gamma_m)$ with dimension $N_m \le \dim(\, W_{0,h}(\gamma_m))$ it's the space to be sought, along with the necessary conditions for this space to replace the standard Lagrange multiplier space defined in (3.2) (when looking for a space to replace the previous one, it is clear why the same name would be chosen). To carry out this task, it is assumed that there exists a basis $\{\, \psi_i \mid 1 \le i \le N_m \,\}$ of the new space $M_{h_m}(\gamma_m)$ such that:

- Exists a positive constant C such that

$$\#(\operatorname{supp}\psi_i) \le C, \quad 1 \le i \le N_m \text{ and } \#(p) \le C, \quad p \in \gamma_m, \tag{3.9}$$

where $\#(\operatorname{supp}\psi_i)$ is the number of elements in S_{m,h_m} having a non-empty intersection with the simply connected support of ψ_i, and $\#(p)$ is the number of basis functions such that the point p is contained in the support of ψ_i;

- Exists a positive constant C such that

$$\begin{aligned} &\forall \mu \in H^{n_m-1/2}(\gamma_m) \quad \exists \mu_\psi \in M_{h_m}(\gamma_m) : \\ &\sum_{e \in S_{m,h_m}} h_e \|\mu - \mu_\psi\|_{0,e}^2 \leq C h_m^{2n_m} |\mu|_{n_m-1/2,\gamma_m}^2 \end{aligned} \tag{3.10}$$

where $\|\cdot\|_{0,e}$ is the L^2-norm on the edge e, $|\cdot|_{n_m-1/2}$ is the $H^{n_m-1/2}(\gamma_m)$ seminorm and h_e is the length of the edge e.

The first one can be considered a property about local support of the basis function; the second one requires that the constants are contained in the Lagrange multiplier space and it's an approximation property of $M_{h_m}(\gamma_m)$.
Now, it's useful define two new basis: the first one is $\{\, \theta_i \mid 1 \leq i \leq M \,\}$, related to a new space $\widetilde{W}_{0,h_m}(\gamma_m)$, subspace of $W_{0,h_m}(\gamma_m)$ defined in (3.8), and the other one is $\{\, \tilde{\theta}_i \mid 1 \leq i \leq M \,\}$ of a new space $\widetilde{W}_{h_m}(\gamma_m)$, subspace of $W_{h_m}(\gamma_m)$ defined in (3.7). Two assumptions about the discrete spaces just introduced and their relation to $M_{h_m}(\gamma_m)$ are made in [29]. The new nonconforming discrete space V_h is defined as in (3.1) using:

$$M_h = \prod_{m=1}^{M} M_{h_m}(\gamma_m) \quad \text{where} \quad M_{h_m}(\gamma_m) = \operatorname{span}\{\, \psi_i \mid 1 \leq i \leq N_m \,\}. \tag{3.11}$$

As pointed out in [29], solutions (u_h, λ_h) and the space V_h depend on the specific choice of basis functions, as well as on the order of the discretization and discretization itself. The reader is directed to the same reference for a priori estimates (same for the "standard" case (3.3)), a study of the consistency error and a discrete inf-sup condition for the stability of the saddle point problem. In summary, the primary benefit of the use of this basis lies in their localized supports. If the first method is adopted, based on the constrained space V_h defined in (3.1), no basis of this space with local support can be constructed [29]. A quick comparison between the Figures 3.2 and 3.3 reveals the two different behaviors, where the non-mortar side is on the left. In the first one, the support of such a nodal basis function on that side is a strip of length $|\gamma_m|$ and width h_m: the locality of the basis functions is lost. In the second one, the value of an element $v \in V_h$ at a point p on the non-mortar side is determined completely by its values in a small neighborhood of p on the mortar side.

In the remainder of this section, some of the basis used in the following chapter will be presented, along with the properties they satisfy. It's important to understand this concept: the first two basis will be constructed directly from ψ_i functions like in (3.11); the third one uses the "dual" approach, i.e. the ψ_i functions depend on some θ_i functions considered.

Starting with $n_k = 1$ for $1 \leq k \leq K$ used in the definition of X_{h_k,n_k}, let's see the first two basis: simply looking at the Figure 3.4 one can easily understand the structure of the basis functions in both cases. M_h^1 is the first space: it's equal to the standard Lagrange multiplier space, where the nodal basis functions

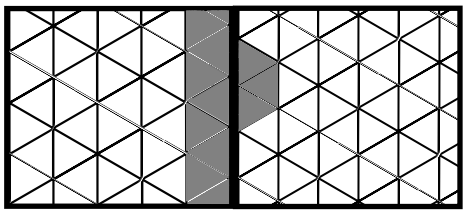

Figure 3.2: Structure of the support of a nodal basis function in V_h in the standard case.

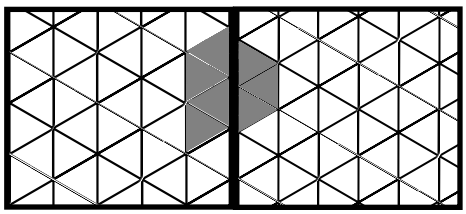

Figure 3.3: Structure of the support of a nodal basis function in V_h in the alternative case.

are continuous and piecewise linear. Basically, there are hat functions in the interior of γ_m, modified only in the neighborhood of two endpoints. The second space M_h^0 (named this way to maintain consistency with the notation used in the article [10]) is based on piecewise constant functions: nodal basis functions are

$$\psi_i(x) = \begin{cases} 1, & x \in \left[\frac{1}{2}(x_{i-1} + x_i), \frac{1}{2}(x_i + x_{i+1})\right], \\ 0, & \text{elsewhere,} \end{cases} \qquad 2 \leq i \leq N_m - 1.$$

Instead, $\psi_1(x)$ and $\psi_{N_m}(x)$ are equal to one on $[x_0, \frac{1}{2}(x_1 + x_2)]$ and $[\frac{1}{2}(x_{N_m-1} + x_{N_m}), x_{N_m+1}]$, respectively, and zero elsewhere. In this context, x_l for $1 \leq l \leq N_m + 1$ are the vertices defined on γ_m. Refer to [29] to see that both these spaces satisfy (3.9) and (3.10).
In the same reference, one can find the definition of two other basis, related with functions $\{\theta_i\}_{i=1}^{N_m}$ and $\{\tilde{\theta}_i\}_{i=1}^{N_m}$ defined before, and therefore referred to as dual basis functions. They are more effective than the previous ones because the locality of the supports of the nodal basis functions of the constrained space is preserved.

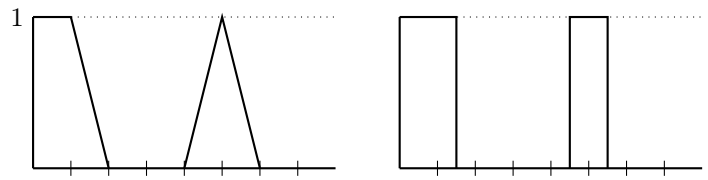

Figure 3.4: Two different types of basis functions for Lagrange multiplier spaces: M_h^1 and M_h^0.

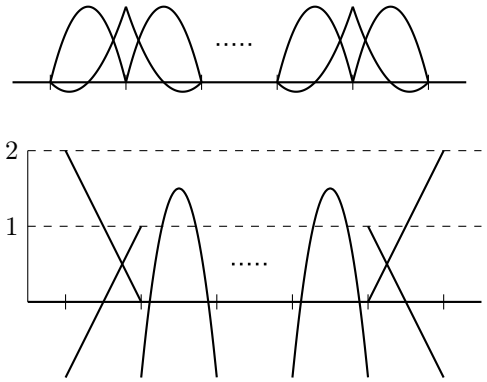

Figure 3.5: Construction of M_h^2: in the upper part, some examples of θ_i; in the lower part, some functions ψ_i.

The final basis M_h^2 that will be used in the implementation part is related to the case where $n_k = 2$ for $1 \leq k \leq K$. The functions ψ_i are defined using the nodal basis functions of standard Lagrange multiplier space $\widetilde{W}_{0,h_m}(\gamma_m)$:

$$\psi_i(x) := \begin{cases} (-1 + \frac{5}{2}\theta_i)(x), & x \in \text{supp } \theta_i, \\ 0, & \text{elsewhere,} \end{cases}$$

and for $i = 2l,\ 2 \leq l \leq (Nm-3)/2$ by:

$$\psi_i(x) := \begin{cases} (\frac{1}{2} - \frac{3}{4}\theta_{i-1} + \theta_i - \frac{3}{4}\theta_{i+1})(x), & x \in \text{supp } \theta_i, \\ 0, & \text{elsewhere.} \end{cases}$$

Differently are defined the first two basis functions, $\psi_1,\ \psi_2$, and the two last ones, $\psi_{Nm-1},\ \psi_{Nm}$:

$$\psi_1(x) := \begin{cases} \frac{2}{h_1}(\|x - x_1\|), & x \in \text{supp } \theta_1, \\ 0, & \text{elsewhere,} \end{cases}$$

$$\psi_2(x) := \begin{cases} \frac{1}{h_1}(\|x - x_0\| - \|x - x_1\|), & x \in \text{supp } \theta_1, \\ (\frac{1}{2} + \theta_2 - \frac{3}{4}\theta_3)(x), & x \in \text{supp } \theta_2 \setminus \text{supp } \theta_1, \\ 0, & \text{elsewhere,} \end{cases}$$

with ψ_{Nm-1} and ψ_{Nm} given in a similar way. Some examples in Figure 3.5. Not only are the conditions (3.9),(3.10) and those mentioned above, related to the dual bases, satisfied, but also a fifth property called biorthogonality:

$$\int_{\gamma_m} \theta_i \psi_j d\sigma = \delta_{ij} c_i \int_{\gamma_m} \theta_i^2 d\sigma, \quad c \leq c_i \leq C, \quad 1 \leq i, j \leq N_m.$$

This allows for maximum locality in the support of the ψ_i on V_h, as shown in Figure 3.3.

3.2 Mortar formulation of the DFN problem

The objective of this section is to define the mortar formulation of the problem derived from Chapter 1 through the use of the virtual element method.
In this context, the polyhedral subdomains of the previous section are the fractures $F_i \subset \mathbb{R}^2$, whose intersection γ_m are the traces. Following mortar terminology, for each $S \in \mathcal{S}$ such that $S = \overline{F}_i \cap \overline{F}_j$, the fracture whose index is such that $m_S(i) = 0$, defined in (1.7), is called *mortar fracture*. The other one is the *non-mortar fracture*. The approximate jump of the co-normal derivative of the solution on the non-mortar side is $\lambda_S = \lambda_{|S}$; on the mortar side, it will be $-\lambda_S$.
The saddle point problem (3.6) is reformulated using the following new spaces, both equipped with (1.14), defined using VEM spaces of order k:

$$V_\delta = \{\, v_\delta \in V_{k,\delta} : \gamma_{\Gamma_i^D}(v_\delta) = 0 \quad \forall i = 1, \dots, N \,\},$$

$$V_\delta^D = \{\, v_\delta \in V_{k,\delta} : \gamma_{\Gamma_i^D}(v_\delta) = \Pi^0_{k,\Gamma^D}(H^D) \quad \forall i = 1, \dots, N \,\},$$

where $\Pi^0_{k,\Gamma^D}(H^D)$ is the piecewise $L^2(e)$ projection on polynomials of degree $\leq k$ for all edges e such that $e \cap \Gamma^D \neq \emptyset$. In this context, V_δ plays the role of X_h in (3.4) and X_{h_k,n_k} is related to $V_{k,\delta}(F_i)$.
Shifting the focus to the Lagrange multiplier space M_h defined in (3.5), $M_{\delta,S} \subset L^2(S)$ is a finite dimensional space, spanned by the basis defined in the last part of the previous section. Thus, $M_{\delta,S}$ is either M_h^0, M_h^1 or M_h^2, created for the trace $S \in \mathcal{S}$. The global space M_h follows:

$$M_\delta \equiv M_h = \prod_{S \in \mathcal{S}} M_{\delta,S}. \tag{3.12}$$

Finally, it is possible to obtain the saddle point problem. Starting from the discrete counterpart of H and Λ, respectively h and λ, the discrete bilinear forms needed are

$$a_{\delta i}(h_i, v_{\delta i}) := \sum_{E \in \tau_{i,\delta}} a_\delta^E(h_{i|E}, v_{\delta i|E}), \quad \forall v_\delta \in V_\delta,$$

where (2.17) is used and $b_i(\cdot,\cdot)$, the one defined in (1.9). The subscript $v_{\delta i}$ indicates the restriction of v_δ at the i-th fracture, the same applies to f_i and h_i. On the right hand side, $(\cdot,\cdot)_\delta$ is defined in (2.24). Finally, the discrete version of (1.15) is: find $h \in V_\delta^D$ such that

$$a_{\delta i}(h_i, v_{\delta i}) + b_i(v_{\delta i}, \lambda) = (f_i, v_{\delta i})_\delta + \left\langle H^N, v_{\delta i} \right\rangle_{\pm\frac{1}{2},\Gamma_i^N} \quad \forall v_\delta \in V_\delta, \quad \forall 1 \leq i \leq N. \tag{3.13}$$

After considering a lifting R_δ^D of $\Pi^0_{k,\Gamma^D}(H^D)$ and the global form $a_\delta(\cdot,\cdot)$ defined in (2.21), summing up (3.13) over all $F_i \subset \Omega$, the saddle point problem finally arises: find $\lambda \in M_\delta$ and $h = h_0 + R_\delta^D$, with $h_0 \in V_\delta$, such that

$$\begin{cases} a_\delta(h_0, v_\delta) + b(v_\delta, \lambda) = (f, v_\delta)_\delta + \left\langle H^N, v_\delta \right\rangle_{\pm\frac{1}{2},\Gamma^N} - a_\delta(R_\delta^D, v_\delta) & \forall v_\delta \in V_\delta, \\ b(h_0, \psi_\delta) = -b(R_\delta^D, \psi_\delta) & \forall \psi_\delta \in M_\delta. \end{cases} \tag{3.14}$$

where $b(\cdot,\cdot)$ is computed as as integral in $L^2(S)$, as in [7].

3.3 Analysis of the discrete problem

As shown in [16], what ensures the well-posedness of a continuous saddle point problem like (1.13) is the coercivity, also known as ellipticity, of the bilinear form $a(\cdot,\cdot)$ and the inf-sup condition associated with the bilinear form $b(\cdot,\cdot)$. However, these properties are not automatically inherited by the discrete counterparts of the two forms, so it is essential to verify them directly in the discrete case. Proposition 2.1 in [16] says that the problem (3.14) is well-posed if $a_\delta(\cdot,\cdot)$ is coercive on the constrained space

$$W_\delta = \{\, v_\delta \in V_\delta : b(v_\delta, \psi_\delta) = 0, \quad \forall \psi_\delta \in M_\delta \,\}$$

and if there exists a positive constant β independent of the discretization parameter δ such that:

$$\inf_{\psi_\delta \in M_\delta} \sup_{v_\delta \in V_\delta} \frac{b(v_\delta, \psi_\delta)}{\|v_\delta\|_V \|\psi_\delta\|_M} \geq \beta. \tag{3.15}$$

The norm $\|\cdot\|_M$ can be chosen between the $H_{00}^{\frac{1}{2}}$ dual norm or a mesh dependent L^2-norm that will be used in the chapter about errors in numerical implementations:

$$\|\psi\|_M = \sum_{S\in\mathcal{S}} \sum_{e\subset S} |e| \|\psi\|_{0;e}^2. \tag{3.16}$$

The notation $\|\cdot\|_{0;e}$ denotes the L^2-norm on the segment e, part of the trace S.

However, a different condition will be requested on $a_\delta(\cdot,\cdot)$. Theorem 3 in [25] states that well-posedness is implied by the discrete condition inf-sup, if the functional $v_\delta \to a_\delta(v_\delta, v_\delta)^{\frac{1}{2}}$ is a norm over W_δ. This leads to the coercivity of the bilinear form, as can be seen in the proof, and the previous cited proposition can be used. The equivalence between $a(\cdot,\cdot)$ and its discrete counterpart stated in (2.22) hints to demonstrate that the functional $v_\delta \to a(v_\delta, v_\delta)^{\frac{1}{2}}$ is a norm over W_δ: then follows that the continue form is coercive with coercivity constant 1, and $a_\delta(\cdot,\cdot)$ is coercive with coercivity constant equal to α_*.

Proposition 3 (see [7]). *Assume that M_δ defined in* (3.12) *contains the functions which are constant on each trace. Then, the functional $v_\delta \to |||v_\delta|||$ is a norm over W_δ where $|||\cdot||| := a(\cdot,\cdot)^{\frac{1}{2}}$.*

Proof. It is sufficient to check that, for all $v_\delta \in W_\delta$,

$$|||v_\delta||| = 0 \iff v_\delta \equiv 0.$$

Clearly, one implication it's obvious. Now, let's take $v_\delta \in W_\delta$ be such that $|||v_\delta||| = 0$. Then it must be constant on each fracture, since its gradient on each fracture is null and the global bilinear form a is made of local bilinear forms a_i, for $1 \leq i \leq N$ (see definition (1.11)). In addition, Dirichlet condition can be used: v_δ vanishes on all fractures F_i such that $\Gamma_i^D \neq \emptyset$. Now, thanks to the network connectivity, v_δ vanishes on all the fractures: let S be a trace shared by fractures F_i and F_j, with $\gamma_S(v_{\delta i}) = 0$.

$$([\![v_\delta]\!]_S, 1)_S = |S| [\![v_\delta]\!]_S = 0 \implies \gamma_S(v_{\delta i}) = \gamma_S(v_{\delta i}) = 0,$$

thanks to the mortar condition, where $(\cdot,\cdot)_S$ clearly indicates the $L^2(S)$-product. Since $v_{\delta i}$ and $v_{\delta j}$ are constant, it follows that $v_{\delta j} = 0$. The other implication is proved, so the Proposition is true. □

Now, let's focus on the discrete inf-sup condition: using Lemma 10 in [25], [9] proves that it's possible to find a positive constant β, independent of the mesh parameter, ideal for that condition in a polynomial Finite Element context on a regular triangulation. The same proof can be used under Assumption 1, made in the VEM chapter, and Assumption 2 below

Assumption 2. *The number of edges of the elements of the discretization* $\tau_\delta = \cup_{i=1}^{N} \tau_{\delta,i}$ *is limited independently of the mesh parameter* δ.

Under Assumption 1, let's consider a trace S, a segment e and E as one of the two polygons that share e that belongs to the discretization of S. Assumption 1 leads to the construction within E of a triangle $T_{e,E}$ that has e as one of its edges, maintaining a shape regularity that depends solely on σ, see Figure 3.6. For instance, since we the elements are convex, this can be achieved by connecting the endpoints of e with the barycenter of E. The area of such a triangle is proportional to the area of E divided by the number of its edges.

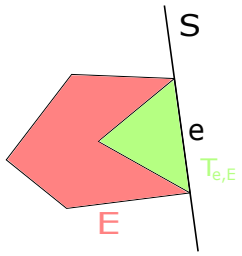

Figure 3.6: An example explaining the consequences of Assumption 1

Thanks to the second assumption, the norm of any function belonging to the finite dimensional space on $T_{e,E}$ is equivalent to the one on E, because the area of the triangle is proportional to the area of the polygon E. Lemma 10 in [25] guarantees the existence of an inf-sup constant independent of δ for $T_{e,E}$ and thus prove the existence of such a constant for E by the equivalence of the norms.

3.4 A priori error estimate

Following [7], the developed theory allows for the derivation of an a priori estimate both for h and λ, respectively the discrete counterpart of the hydraulic head H and of the flux Λ. Using (2.24), the operators $\mathcal{F}, \mathcal{F}_\delta \in V'$ defined below will be useful in this context:

$$\langle \mathcal{F}, v \rangle_{\pm 1,\Omega} := (f, v)_\Omega, \quad \langle \mathcal{F}_\delta, v \rangle_{\pm 1,\Omega} := (f, v)_\delta, \tag{3.17}$$

together with

$$W_\delta^D = \{v \in V_\delta^D : b(v, \psi) = 0, \quad \forall \psi \in M_\delta\},$$
$$\mathbb{P}_k^D(\Omega) = \{p \in V_\delta^D : p \in \mathbb{P}_k(E), \quad \forall E \in \tau_\delta\}.$$

Let's prove a preliminary result, assuming the hypothesis of Proposition 1 holds.

Lemma 1 (Poincarè's inequality in a DFN, [7]). *Let's define the space* $\widetilde{W} = \{ v \in V : \int_S [\![v]\!] = 0, \quad \forall S \in \mathcal{S} \}$. *Then, exists a positive constant* C_Ω *such that for all* $w \in \widetilde{W}$*:*

$$\left(\sum_{i=1}^{N} \|w\|^2_{L^2(F_i)} \right)^{\frac{1}{2}} \leq C_\Omega |||w|||. \tag{3.18}$$

Proof. The proof of the previous proposition can be applied to prove that $|||\cdot|||$ is a norm on $\widetilde{W}$. This implies that the right-hand side of (3.18) does vanish if and only if $w \in \widetilde{W}$ is identically zero. By contradiction, suppose

$$\forall C > 0, \ \exists w_C \in \widetilde{W} : \ \|w_C\|_\Omega := \left(\sum_{i=1}^{N} \|w_C\|^2_{L^2(F_i)} \right)^{\frac{1}{2}} > C|||w_C|||.$$

A sequence of functions can be considered:

$$w_k \in \widetilde{W}, k \in \mathbb{N}, \quad \text{such that} \quad \|w_k\|_\Omega > k|||w_k|||.$$

Without loss of generality, let's suppose that this function are unitary in Ω-norm.
Then, it's easy to see $\|w_k\|_{H^1(F_i)}$ is limited for all $i = 1, \dots, N$. In fact,

$$\|w_k\|^2_{H^1(F_i)} = \|w_k\|^2_{L^2(F_i)} + \|\nabla w_k\|^2_{L^1(F_i)}$$

and the first part is limited thanks to $\|w_k\|_\Omega = 1$, the second one since $|||w_k|||^2 = \sum_{i=1}^N \|\nabla w_k\|_{L^2(F_i)}$ is limited. Reflexivity of V, closed in $H^1(\Omega)$, allows for the identification of a function w^* that is a weak limit of the sequence, up to subsequences. Clearly, ∇w_k converges to ∇w^* weakly.
Let's prove that

$$\|\nabla w^*\|_{L^2(F_i)} = 0.$$

In fact, since

$$0 \leq \|\nabla w_k - \nabla w^*\|^2_{L^2(F_i)} = \|\nabla w_k\|^2_{L^2(F_i)} - 2\langle \nabla w_k, \nabla w^* \rangle_{L^2(F_i)} + \|\nabla w^*\|^2_{L^2(F_i)}, \tag{3.19}$$

and, using the definition of the triple norm (see Proposition 3),

$$1 < k|||w_k||| \implies \|\nabla w_k\|^2_{L^2(F_i)} < \frac{1}{k},$$

taking the limit for $k \to \infty$ in (3.19), it follows that $\|\nabla w^*\|_{L^2(F_i)} = 0$.
Then, w^* is constant on each fracture and, by the same arguments used in the proof of Proposition 3, it follows that $w^* \equiv 0$. Moreover, since $H^1(F_i)$ is compactly embedded in $L^2(F_i)$, w_k converges strongly to w^* in $L^2(F_i)$ for all the fractures F_i. Since $\|w_k\|_{L^2(F_i)} \xrightarrow{k\to\infty} \|w^*\|_{L^2(F_i)}$ for all $i = 1, \dots, N$, a contradiction is obtained: $\|w_k\|_{l_2} = 1$. □

An a priori error estimate can now be proved.

Theorem 1 (see [7]). *Let $V_\delta, M_\delta, W_\delta, W_\delta^D$ and $\mathbb{P}_k^D(\Omega)$ be as previously defined. Then, the solution (h, λ) to problem (3.14) and the solution (H, Λ) to problem (1.13) satisfy*

$$\begin{aligned}|||H-h||| \leq \left(1+\frac{\alpha^*}{\alpha_*}\right) \inf_{v_\delta \in W_\delta^D} |||H-v_\delta||| + \frac{1+\alpha^*}{\alpha_*} \inf_{p_k \in \mathbb{P}_k^D(\Omega)} |||H-p_k||| \\ + \frac{1}{\alpha_*}\left(\inf_{\psi_\delta \in M_\delta} \sup_{v_\delta \in W_\delta} \frac{b(v_\delta, \Lambda-\psi_\delta)}{|||v_\delta|||}\right) + \frac{1+C_\Omega}{\alpha_*}\|\mathcal{F}-\mathcal{F}_\delta\|_{V'}.\end{aligned}$$

If the discrete inf-sup condition (3.15) holds, then

$$\begin{aligned}\|\Lambda-\lambda\|_M \leq \left(1+\frac{1}{\beta}\right) \inf_{\psi_\delta \in M_\delta} \|\Lambda-\psi_\delta\|_M + \frac{\sqrt{\alpha^*}}{\beta}|||H-h||| \\ + \frac{1+\sqrt{\alpha^*}}{\beta} \inf_{p_k \in \mathcal{P}_k^D(\Omega)} \|H-p_k\| + \frac{1}{\beta}\|\mathcal{F}-\mathcal{F}_\delta\|_{V'}.\end{aligned}$$

Following [25] for the proof, a special norm on M must be introduced:

$$\|\mu\|_M := \sup_{v_\delta \in V_\delta} \frac{b(v_\delta, \mu)}{\|v_\delta\|_V}. \tag{3.20}$$

Proof. Firstly, take an arbitrary function $h_l \in W_\delta^D$ and an arbitrary polynomial function $p \in \mathbb{P}_k^D$. Define $\delta_l := h_l - h$. Thanks to the equations of the saddle point problems (1.13), (3.14) and the property of *k-Consistency* (2.18) (this clearly reflects on the global discrete bilinear form $a_\delta(\cdot,\cdot)$ defined in (2.21)):

$$\begin{aligned}a_\delta(\delta_l, \delta_l) &\overset{\text{bilinearity}}{=} a_\delta(h_l - p, \delta_l) + a_\delta(p, \delta_l) - a_\delta(h, \delta_l) \\ &\overset{(2.18),\ (3.14)}{=} a_\delta(h_l - p, \delta_l) + a(p, \delta_l) - [(f, \delta_l)_\delta - b(\delta_l, \lambda) + \langle H^N, \delta_l\rangle_{\Gamma^N}] \\ &\overset{\text{bilinearity}}{=} a_\delta(h_l - p, \delta_l) + a(p - H, \delta_l) + a(H, \delta_l) - [(f, \delta_l)_\delta - b(\delta_l, \lambda) \\ &\qquad + \langle H^N, \delta_l\rangle_{\Gamma^N}] \\ &\overset{(1.13)}{=} a_\delta(h_l - p, \delta_l) + a(p - H, \delta_l) + a(H, \delta_l) - (f, \delta_l)_\delta + b(\delta_l, \lambda) \\ &\qquad + (f, \delta_l) - b(\delta_l, \Lambda) \\ &\overset{\delta_l \in W_\delta}{=} a_\delta(h_l - p, \delta_l) + a(p - H, \delta_l) - (f, \delta_l)_\delta + (f, \delta_l) - b(\delta_l, \Lambda).\end{aligned}$$

In fact, $\delta_l \in W_\delta$ since $h, h_l \in W_\delta^D$, so $\gamma_{\Gamma_i^D}(\delta_l) = 0$. This fact allows the use of (1.13) and (3.14), since δ_l equal to zero in the Dirichlet border. Consider a generical $\psi_\delta \in M_\delta$, so $b(\delta_l, \psi_\delta) = 0$ by definition. Then, continuing the equality,

$$a_\delta(\delta_l, \delta_l) \overset{\text{Def.}\ (3.17)}{=} a_\delta(h_l - p, \delta_l) + a(p - H, \delta_l) - \langle \mathcal{F} - \mathcal{F}_\delta, \delta_l\rangle_{\pm 1,\Omega} - b(\delta_l, \Lambda).$$

Using the continuity of $a(\cdot,\cdot)$ with norm 1 with respect to the norm induced by itself, i.e.

$$a(h_l - p, \delta_l) \leq |a(h_l - p, \delta_l)| \leq |||h_l - p|||\,|||\delta_l|||,$$

it's obtained the continuity of its discrete counterpart with continuity constant equal to α^* using (2.22). Then, using a consequence of the triangle inequality

($|u-v| \leq |u| + |v|$) and $b(\delta_l, \psi_\delta) = 0$, it's possible to proceed with the previous relation:

$$a_\delta(\delta_l, \delta_l) \leq \Big(\alpha^* |||h_l - p||| + |||H - p||| + \frac{b(\delta_l, \Lambda - \psi_\delta)}{|||\delta_l|||}\Big)|||\delta_l||| + \|\mathcal{F} - \mathcal{F}_\delta\|_{V'}\|\delta_l\|_V.$$

In fact, the triangle inequality is used with $u = a_\delta(\cdot,\cdot) + a(\cdot,\cdot) + \langle\cdot,\cdot\rangle$ and $v = b(\cdot,\cdot)$. Then, thanks to the previous lemma and the definition of the V-norm in (1.14),

$$\|\delta_l\|_V^2 = \sum_{i=1}^N \|(\delta_l)_{|i}\|_{L^2(F_i)}^2 + \sum_{i=1}^N \big|\big|\big|\nabla(\delta_l)_{|i}\big|\big|\big|_{F_i}^2 \leq (1 + C_\Omega^2)|||\delta_l|||^2$$

$$\implies \|\delta_l\|_V \leq \sqrt{(1 + C_\Omega^2)}|||\delta_l||| \leq (1 + C_\Omega^2)|||\delta_l|||.$$

Finally,

$$a_\delta(\delta_l, \delta_l) \leq \Big(\alpha^* |||h_l - p||| + |||H - p||| + \frac{b(\delta_l, \Lambda - \psi_\delta)}{|||\delta_l|||} + (1 + C_\Omega^2)\|\mathcal{F} - \mathcal{F}_\delta\|_{V'}\Big)|||\delta_l|||. \tag{3.21}$$

Now, let $h_l \in W_\delta^D$ be the a-orthogonal projection of $H \in V^D$ over W_δ^D, i.e.

$$a(H - h_l, v_\delta) = 0, \quad \forall v_\delta \in W_\delta^D,$$

so, it's true that:

$$|||H - h|||^2 = |||H - h_l|||^2 + |||\delta_l|||^2 = \Big(\inf_{v_\delta \in W_\delta^D} |||H - v_\delta|||\Big)^2 + |||\delta_l|||^2. \tag{3.22}$$

The first inequality of the Theorem is finally obtained from:

$$\begin{aligned} |||\delta_l|||^2 = a(\delta_l, \delta_l) &\leq \frac{1}{\alpha_*} a_\delta(\delta_l, \delta_l) \\ &\leq \frac{1}{\alpha_*}\Big(\alpha^* |||h_l - p||| + |||H - p||| + \frac{b(\delta_l, \Lambda - \psi_\delta)}{|||\delta_l|||} \\ &\quad + (1 + C_\Omega^2)\|\mathcal{F} - \mathcal{F}_\delta\|_{V'}\Big)|||\delta_l|||. \end{aligned}$$

$$\implies |||\delta_l||| \leq \frac{1}{\alpha_*}\Big(\alpha^* |||h_l - p||| + |||H - p||| + \frac{b(\delta_l, \Lambda - \psi_\delta)}{|||\delta_l|||} + (1 + C_\Omega^2)\|\mathcal{F} - \mathcal{F}_\delta\|_{V'}\Big).$$

In fact, since $\sqrt{(x^2 + y^2)} \leq x + y$ if x, y are positive, then from (3.22), and taking the supremums and infimums in (3.21),

$$\begin{aligned} |||H - h||| &\leq \Big(\inf_{v_\delta \in W_\delta^D} |||H - v_\delta|||\Big) + |||\delta_l||| \\ &\leq \left(1 + \frac{\alpha^*}{\alpha_*}\right) \inf_{v_\delta \in W_\delta^D} |||H - v_\delta||| + \frac{1 + \alpha^*}{\alpha_*} \inf_{p_k \in \mathbb{P}_k^D(\Omega)} |||H - p_k||| \\ &\quad + \frac{1}{\alpha_*}\left(\inf_{\psi_\delta \in M_\delta} \sup_{v_\delta \in W_\delta} \frac{b(v_\delta, \Lambda - \psi_\delta)}{|||v_\delta|||}\right) + \frac{1 + C_\Omega^2}{\alpha_*}\|\mathcal{F} - \mathcal{F}_\delta\|_{V'}. \end{aligned}$$

This is the desired inequality, except for redefining the constant C_Ω.

Let's now focus on the second inequality. Taking an arbitrary $\psi_\delta \in M_\delta$ and an arbitrary $p \in \mathbb{P}_k^D(\Omega)$

$$\begin{aligned}\beta\|\psi_\delta-\lambda\|_M &\overset{(3.15)}{\leq} \sup_{v_\delta\in V_\delta} \frac{b(v_\delta,\psi_\delta-\lambda)}{\|v_\delta\|_V} = \sup_{v_\delta\in V_\delta} \frac{b(v_\delta,\Lambda-\lambda)+b(v_\delta,\psi_\delta-\Lambda)}{\|v_\delta\|_V}\\ &\overset{(1.13),\,(3.14)}{\leq} \sup_{v_\delta\in V_\delta} \frac{a_\delta(h,v_\delta)-(f,v_\delta)_\delta-a(H,v_\delta)+(f,v_\delta)+b(v_\delta,\psi_\delta-\Lambda)}{\|v_\delta\|_V}\end{aligned}$$

$$\overset{(2.18)}{\leq} \sup_{v_\delta\in V_\delta} \frac{a_\delta(h-p,v_\delta)_\delta+a(p-H,v_\delta)+\langle\mathcal{F}-\mathcal{F}_\delta,v_\delta\rangle_V+b(v_\delta,\psi_\delta-\Lambda)}{\|v_\delta\|_V}.$$

Clearly, using the continuity of $a(\cdot,\cdot)$ with respect to triple norm , and a Cauchy-Schwartz inequality on its discrete counterpart, it's possible to proceed with

$$\begin{aligned}\beta\|\psi_\delta-\lambda\|_M &\leq \sup_{v_\delta\in V_\delta} \frac{\sqrt{a_\delta(h-p,h-p)a_\delta(v_\delta,v_\delta)}+b(v_\delta,\psi_\delta-\Lambda)}{\|v_\delta\|_V}\\ &\quad+|||H-p|||+\|\mathcal{F}-\mathcal{F}_\delta\|_{V'}\\ &\overset{(3.20)}{\leq} \sqrt{\alpha^*}|||h-p|||+|||H-p|||+\|\mathcal{F}-\mathcal{F}_\delta\|_{V'}+\|\Lambda-\psi_\delta\|_M\\ &\leq \sqrt{\alpha^*}|||H-h|||+(1+\sqrt{\alpha^*})|||H-p|||+\|\mathcal{F}-\mathcal{F}_\delta\|_{V'}+\|\Lambda-\psi_\delta\|_M.\end{aligned}$$

The proof is concluded by the triangle inequality and taking the infimum over $\mathbb{P}_k^D(\Omega)$. □

Chapter 4

Implementation and numerical results

Following the correspondent sections in [10, 11, 12], in this chapter it will be showed how to implement the mixed VEM-Mortar method. In addition, some numerical results will be analyzed to understand the practical behavior of the method. In this chapter, a quick overview of the creation of the working mesh is provided (Section 4.1), enriched by a description of the mesh smoothing process, then the algebraic formulation of the problem with a detailed analysis of the matrices involved can be found in Section 4.2, and finally, the numerical results obtained by applying the mixed VEM-Mortar method to a DFN with three fractures are presented in Section 4.3.

4.1 Mesh generation

The procedure for obtaining the computational mesh on the fracture network is first described. This technique is carried out independently for each fracture, without considering trace locations or positions. Initially, a good quality triangulation is created for each fracture, which does not necessarily conform to the trace arrangement and is generated independently for each fracture F_i. This is called *base mesh*. In the second step, a local conforming mesh is produced, where the triangles of the *base mesh* are subdivided into polygons that align with the traces. However, it should be noted that elements from meshes of different fractures result in distinct discretizations of the same trace, as indicated in Section 3.1. This mesh is called *VEM mesh* and is created as follows [10, 11, 12]. Every time a trace intersects an edge of the triangulation, a new node is added at the intersection point. Additional nodes are placed at the ends of traces (trace tips). If a trace tip lies within a triangular element, the geometric segment representing the trace is extended to reach the closest edge of the triangulation, creating a new edge and node in the process. When two traces cross each other, they are divided into two sub-traces, and a new node is created at their intersection point. Finally, traces that lack internal nodes are assigned a new node at their midpoint, which is required to define the discrete Mortar space for the trace.

A problem can appear, since the final mesh may not align with what is

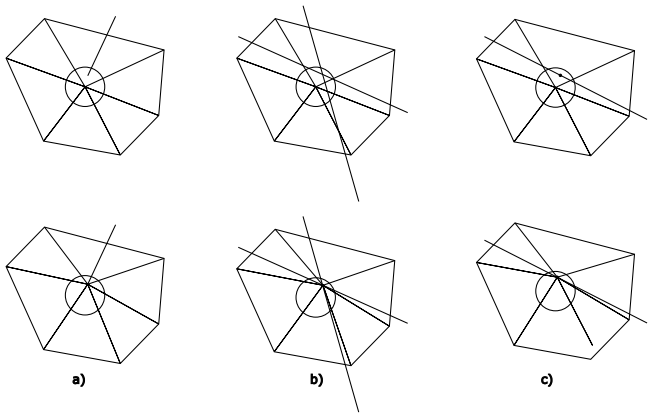

Figure 4.1: Mesh smoothing process

requested by Assumption 1, while Assumption 2 is always verified (see [10]). In order to improve the quality of the *VEM mesh*, a mesh smoothing process can be introduced as described in [10]: let's introduce for each vertex a quantity r_m called *moving radius*, defined as a fixed rate of the smallest edge connected to that vertex, and a quantity called *moving ball*, defined as a ball with center the vertex and radius equal to r_m. With these objects, let's perform a three steps strategy that consists on the shift of some vertex of the *VEM mesh*:

a) if a moving ball of a vertex contains a trace tip, the vertex is moved on the tip;

b) if a moving ball of a vertex not previously moved contains a two traces intersection, the vertex is moved on the intersection;

c) if a moving ball of a vertex not previously moved contains a trace, the vertex is moved orthogonally on that trace.

Refer to Figure 4.1 for each of the steps described before. An example of a mesh creation is proposed in Figure 4.2.

4.2 Matrix formulation of the problem

In order to analyze how is implemented the discrete problem (3.14), let's see an efficient and optimized computation of projectors and local matrices, a key issue for VEM application to large scale problems. A first example of how projectors can be implemented can be found in [6]. Here it's proposed a matrix-based order indipendent implementation of the above framework, following the steps of the saddle point problem in [10].

Each trace $S \in \mathcal{S}$ is discretized following the triangulation on the respective non-mortar fracture: a finite dimensional subspace of dimension N^S, containing the constant functions (as required by Proposition 3), is introduced, see (3.12).

As in Section 2.1, consider a fracture $F_i \subset \mathbb{R}^2$ and the *VEM mesh* $\tau_{\delta,i}$, created using the steps outlined in the previous section. The number of DOFs on the boundary of a generic element $E \in \tau_{\delta,i}$ are denoted by $N_{\text{dof}}^{\partial E}$, named

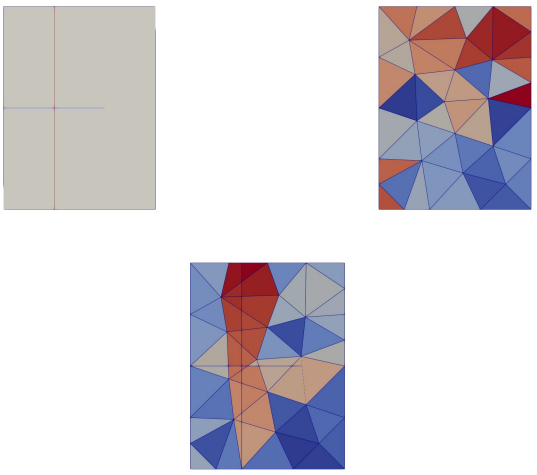

Figure 4.2: A domain with 2 traces with the respective *base mesh* and *VEM mesh*. The coloring of the cells corresponds to their index.

boundary dofs, and the number of DOFs on the internal of E are denoted by N°_{dof}, named *internal dofs*. Recalling (D1)-(D2)-(D3) in Section 2.1 and the notation used there,

$$N^{\partial E}_{\text{dof}} = kn_v, \quad N^{\circ}_{\text{dof}} = \frac{k(k-1)}{2}, \quad N^{E}_{\text{dof}} := N^{\partial E}_{\text{dof}} + N^{\circ}_{\text{dof}},$$

and the $k+1$ quadrature points in (D1)-(D2) are denoted by $\{\, x_j^{\partial E} \,\}_{j=1}^{N^{\partial E}_{\text{dof}}}$. Furthermore from (2.5), let's distinguish between *boundary basis functions*, φ_i^{∂}, $i \in \{\, 1, \dots, N^{\partial E}_{\text{dof}} \,\}$, and *internal basis functions*, φ_i°, $i \in \{\, N^{\partial E}_{\text{dof}} + 1, \dots, N^{E}_{\text{dof}} \,\}$:

$$\varphi_i^{\partial}(x_j^{\partial E}) = \delta_{ji} \quad \forall j \in \{1, \dots, N^{\partial E}_{\text{dof}}\}, \quad (\varphi_i^{\partial}, m_j)_E = 0 \quad \forall j \in \{1, \dots, n_{k-2}\}, \tag{4.1}$$

$$\varphi_i^{\circ}(x_j^{\partial E}) = 0 \quad \forall j \in \{1, \dots, N^{\partial E}_{\text{dof}}\}, \quad (\varphi_i^{\circ}, m_j)_E = |E|\delta_{ji} \quad \forall j \in \{1, \dots, n_{k-2}\}, \tag{4.2}$$

where $n_{k-2} := \dim(\mathbb{P}_{k-2}(E))$.

As is widely known, in order to analyze the implementation of the method, quadrature points $\mathcal{Q}(E) := \{\, x_i^E \,\}_{i=1}^{N^E_{\mathcal{Q}}}$ and weights $\mathcal{W}(E)$ on $E \in \tau_{\delta,i}$ must be defined, together with quadrature points $\mathcal{Q}(\partial E) := \{\, x_i^{\partial E} \,\}_{i=1}^{N^{\partial E}_{\mathcal{Q}}}$ and weights $\mathcal{W}(\partial E)$ on ∂E. From these definitions, jumps out that:

$$N^E_{\mathcal{Q}} := \#\mathcal{Q}(E) = \#\mathcal{W}(E) \quad \text{and} \quad N^{\partial E}_{\mathcal{Q}} := \#\mathcal{Q}(\partial E) = \#\mathcal{W}(\partial E).$$

Although the points corresponding to the Lagrangian degrees of freedom on the edges could be selected independently from the quadrature points on ∂E, for computational efficiency in the VEM projectors, the quadrature points on the boundary are derived by mapping the $k+1$ Gauss-Lobatto quadrature points (with algebraic order $2k-1$) defined on a reference interval $\hat{e}$ onto each edge. The reference points and weights are denoted by $\hat{x}_l, \hat{w}_l$ with $l \in \{\, 1, \dots, k+1 \,\}$.

Now that the context of the local DOFs has been defined for both the VEM and the Mortar part of the problem, let N_h and N_λ be the total number of DOFs for h and λ, defined in Section 3.2. Then, let's denote by ϕ_k, $k = 1, \dots, N_h$, and ψ_l, $l = 1, \dots, N_\lambda$, the basis functions for h and λ, respectively. The number of functions ϕ_j^D used to create R^D, the lifting of the Dirichlet boundary condition, is N^D. Then, the discrete problem (3.14) can be written $\forall k = 1, \dots, N_h$ and $\forall m = 1, \dots, N_\lambda$ as

$$\sum_{j=1}^{N_h} a_\delta(\phi_j, \phi_k) h_j + \sum_{l=1}^{N_\lambda} b(\phi_k, \psi_l)\lambda_l = (f, \phi_k)_\delta + (H^N, \phi_k)_{\Gamma^N} - \sum_{j=1}^{N^D} a_\delta(\phi_j^D, \phi_k) h_j^D,$$

$$\sum_{j=1}^{N_h} b(\phi_j, \psi_m) h_j = -\sum_{j=1}^{N^D} b(\phi_j^D, \psi_m) h_j^D,$$

where h_j^D is the value of $\Pi^0_{k,\Gamma^D}(H^D)$ at the boundary node corresponding to ϕ_j^D. The following linear system is the final product of the discretization method:

$$\begin{pmatrix} \mathbf{A} \in \mathbb{R}^{N_h \times N_h} & \mathbf{B} \in \mathbb{R}^{N_h \times N_\lambda} \\ \mathbf{B}^T \in \mathbb{R}^{N_\lambda \times N_h} & \mathbf{0} \in \mathbb{R}^{N_\lambda \times N_\lambda} \end{pmatrix} \begin{pmatrix} \mathbf{h} \\ \boldsymbol{\lambda} \end{pmatrix} = \begin{pmatrix} \mathbf{F} \\ \boldsymbol{\Psi} \end{pmatrix}, \tag{4.3}$$

where, $\forall k, j = 1, \dots, N_h, \forall m = 1, \dots, N_\lambda$,

$$A_{kj} := a_\delta(\phi_j, \phi_k), \quad B_{jm} := b(\phi_j, \psi_m),$$

$$F_k := (f, \phi_k)_\delta + (H^N, \phi_k)_{\Gamma^N} - \sum_{j=1}^{N^D} a_\delta(\phi_j^D, \phi_k) h_j^D, \quad \Psi_m := -\sum_{j=1}^{N_\phi} b(\phi_j^D, \psi_m) h_j^D.$$

$$h_k := k\text{-th DOF of } h, \quad \lambda_m := m\text{-th DOF of } \lambda.$$

Remark 7. *In the construction of matrix* $\mathbf{A}$*, the choice of trace type becomes evident: as mentioned in Remark 3, a VEM trace, compared to a mortar trace, only implies that instead of a diagonal block for each fracture, there are diagonal blocks shared among fractures that share a VEM trace.*

As mentioned briefly in the VEM chapter, in order to construct discrete forms as (2.21) and (2.25), local forms must be built using polynomial projections of the basis functions (2.5). Here is proposed an approach related to [6], which, for any $E \in \tau_{\delta,i}$, computes the matrix counterpart $\mathbf{\Pi}^*_{E,k} \in \mathbf{R}^{n_k \times N^E_{\text{dof}}}$ to the polynomial projector $\Pi^*_{E,k} : V_{k,\delta}(E) \to \mathbb{P}_k(E)$ such that

$$\text{dof}_{\mathbb{P}_k(E)} \left(\Pi^*_{E,k}(v_\delta) \right) = \mathbf{\Pi}^*_{E,k} \, \text{dof}_{V_{k,\delta}(E)} \left(v_\delta \right), \quad \forall v_\delta \in V_{k,\delta}(E), \tag{4.4}$$

where $\text{dof}_*(\cdot)$ is the operator returning the vector of degrees of freedom in the specified space $*$. Basically, (2.4) here is indicated as $\text{dof}_{V_{k,\delta}(E)}(\cdot)$.

4.2.1 Preliminary matrices

Some matrices and vectors are needed in the preliminary.

- Monomial Vandermonde matrix of order k, denoted by $\mathbf{V}_k^E \in \mathbb{R}^{N_{\mathcal{Q}}^E \times n_k}$

$$(\mathbf{V}_k^E)_{ij} := m_j(x_i^E), \quad i \in \{1, \dots, N_{\mathcal{Q}}^E\}, j \in \{1, \dots, n_k\}. \tag{4.5}$$

  m_j are defined in (2.1) using Table 2.1 for indexing;

- quadrature weights vector

$$\mathbf{w}^E \in \mathbb{R}^{N_{\mathcal{Q}}^E}; \tag{4.6}$$

- diagonal quadrature weights matrix $\mathbf{W}^E \in \mathbb{R}^{N_{\mathcal{Q}}^E} \times \mathbb{R}^{N_{\mathcal{Q}}^E}$

$$(\mathbf{W}^E)_{ij} := (\mathbf{w}^E)_i \delta_{ij}, \quad i, j \in \{1, \dots, N_{\mathcal{Q}}^E\}; \tag{4.7}$$

- monomial Vandermonde matrix of order k, denoted by $\mathbf{V}_k^{\partial E} \in \mathbb{R}^{N_{\mathcal{Q}}^{\partial E} \times n_k}$

$$(\mathbf{V}_k^{\partial E})_{ij} := m_j(x_i^{\partial E}), \quad i \in \{1, \dots, N_{\mathcal{Q}}^{\partial E}\}, j \in \{1, \dots, n_k\}. \tag{4.8}$$

  m_j are defined in (2.1) using Table 2.1 for indexing;

- quadrature weights vector $\mathbf{w}^{\partial E} \in \mathbb{R}^{N_{\mathcal{Q}}^{\partial E}}$, defined for each polygon vertex as the sum of the quadrature weights of the vertex for each edge concurring in the vertex suitably rescaled with the length of the edge. Basically, having $\hat{w}_l$ as the reference quadrature weight associated to the i-th point (global index in the set of boundary quadrature points on ∂E) and $|\hat{e}|$ as the length of the quadrature reference interval, then

$$\left(\mathbf{w}^{\partial E}\right)_i := \frac{\hat{w}_\ell}{|\hat{e}|} \sum_{\substack{e \text{ edge of } E \\ x_i \in e}} |e|; \tag{4.9}$$

- diagonal quadrature weights matrix $\mathbf{W}^{\partial E} \in \mathbb{R}^{N_{\mathcal{Q}}^{\partial E}} \times \mathbb{R}^{N_{\mathcal{Q}}^{\partial E}}$

$$(\mathbf{W}^{\partial E})_{ij} := (\mathbf{w}^{\partial E})_i \delta_{ij}, \quad i, j \in \{1, \dots, N_{\mathcal{Q}}^{\partial E}\}; \tag{4.10}$$

- $\mathbf{w}_x^{\partial E} \in \mathbb{R}^{N_{\mathcal{Q}}^{\partial E}}$, $\mathbf{w}_y^{\partial E} \in \mathbb{R}^{N_{\mathcal{Q}}^{\partial E}}$. Let $\hat{\mathbf{n}}_e = (\hat{n}_{e,x}, \hat{n}_{e,y})$ be the unit vector orthogonal to e edge of E and pointing outward from E and the i-th boundary quadrature point the corresponding for the l-th reference point, then

$$\left(\mathbf{w}_*^{\partial E}\right)_i := \frac{\hat{w}_\ell}{|\hat{e}|} \sum_{\substack{e \text{ edge of } E \\ x_i \in e}} |e| \hat{n}_{e,*}, \quad i \in \{1, \dots, N_{\mathcal{Q}}^{\partial E}\}, \quad * \in \{x, y\}; \tag{4.11}$$

- diagonal quadrature matrices $\mathbf{W}_x^{\partial E} \in \mathbb{R}^{N_{\mathcal{Q}}^{\partial E}} \times \mathbb{R}^{N_{\mathcal{Q}}^{\partial E}}$, $\mathbf{W}_y^{\partial E} \in \mathbb{R}^{N_{\mathcal{Q}}^{\partial E}} \times \mathbb{R}^{N_{\mathcal{Q}}^{\partial E}}$

$$\left(\mathbf{W}_*^{\partial E}\right)_{ij} := \left(\mathbf{w}_*^{\partial E}\right)_i \delta_{ij}, \quad i, j \in \{1, \dots, N_{\mathcal{Q}}^{\partial E}\}, \quad * \in \{x, y\}; \tag{4.12}$$

- preliminary matrices of coefficients implied in the derivatives of monomials $\mathbf{D}_{k,x}, \mathbf{D}_{k,y} \in \mathbb{R}^{n_k \times n_k}$. Given j index of a scaled monomial (Table 2.1) of index $\boldsymbol{\alpha} = (\alpha_x, \alpha_y)$, can be easily seen that:

$$\frac{\partial m_j}{\partial x} = \frac{\alpha_x}{h_E} m_i \quad \text{with} \quad i = j - \alpha_x - \alpha_y, \quad \text{if } \alpha_x > 0,$$

$$\frac{\partial m_j}{\partial y} = \frac{\alpha_y}{h_E} m_i \quad \text{with} \quad i = j - \alpha_x - \alpha_y - 1, \quad \text{if } \alpha_y > 0,$$

  while in the other cases the derivative is null. h_E is set as the diameter of E. These two matrices collects such coefficients: for all $j \in \{1, \dots, n_k\}$ like before

$$(\mathbf{D}_{k,x})_{ij} := \begin{cases} \alpha_x & \text{if } i = j - \alpha_x - \alpha_y \text{ and } \alpha_x > 0, \\ 0 & \text{otherwise,} \end{cases} \tag{4.13}$$

$$(\mathbf{D}_{k,y})_{ij} := \begin{cases} \alpha_y & \text{if } i = j - \alpha_x - \alpha_y - 1 \text{ and } \alpha_y > 0, \\ 0 & \text{otherwise;} \end{cases} \tag{4.14}$$

- modified preliminary matrices $\mathbf{D}^E_{k,x}, \mathbf{D}^E_{k,y} \in \mathbb{R}^{n_k \times n_k}$ equals to

$$\mathbf{D}^E_{k,*} := \frac{1}{h_E} \mathbf{D}_{k,*}, \quad * \in \{x, y\}.$$

  So, it's true that:

$$\frac{\partial m_j}{\partial *} = \sum_{i=1}^{n_k} (\mathbf{D}^E_{k,*})_{ij} m_i, \quad * \in \{x, y\};$$

- Vandermonde matrices of derivatives of monomials $\mathbf{V}^E_{k,x}, \mathbf{V}^E_{k,y} \in \mathbb{R}^{N^E_{\mathcal{Q}} \times n_k}$

$$\mathbf{V}^E_{k,*} := \mathbf{V}^E_k \mathbf{D}^E_{k,*}, \quad * \in \{x, y\}. \tag{4.15}$$

  Since the first column of the preliminary matrices $\mathbf{D}_{k,x}, \mathbf{D}_{k,y}$ is null, the first column of $\mathbf{V}^E_{k,x}, \mathbf{V}^E_{k,y}$ is null, as expected.

- gradient matrix $\boldsymbol{\nabla}^E_k \in \mathbb{R}^{2n_k \times n_k}$

$$\boldsymbol{\nabla}^E_k := \begin{bmatrix} \mathbf{D}^E_{k,x} \\ \mathbf{D}^E_{k,y} \end{bmatrix};$$

- Laplace matrix $\mathbf{L}_k \in \mathbb{R}^{n_k \times n_k}$

$$\mathbf{L}_k := (\boldsymbol{\nabla}^E_k)^T \boldsymbol{\nabla}^E_k = (\mathbf{D}^E_{k,x})^2 + (\mathbf{D}^E_{k,y})^2;$$

- modified Laplace matrix $\mathbf{L}^E_k \in \mathbb{R}^{n_k \times n_k}$

$$\mathbf{L}^E_k := \frac{1}{h^2_E} \mathbf{L}_k;$$

- Vandermonde matrix of the Laplace operator applied to monomials $\mathbf{V}^E_{k,\Delta} \in \mathbb{R}^{N^E_{\mathcal{Q}} \times n_k}$

$$\mathbf{V}^E_{k,\Delta} := \mathbf{V}^E_k \mathbf{L}^E_k; \tag{4.16}$$

4.2.2 Projector matrices

The first projector is the H^1-orthogonal projection $\Pi^{\nabla}_{E,k}(\cdot)$ defined in (2.7). Using scaled monomials (2.1) as a basis for $\mathbb{P}_k(E)$, the vector of DOFs of $\Pi^{\nabla}_{E,k}(\varphi_l)$, where φ_l are defined in (2.5) and (4.1)-(4.2) for $l = 1, \dots, N^E_{\text{dof}}$, satisfies

$$\sum_{j=1}^{n_k} (\nabla m_j, \nabla m_i)_E \left(\text{dof}_{\mathbb{P}_k(E)}(\Pi^{\nabla}_{E,k}(\varphi_l))\right)_j = (\nabla \varphi_l, \nabla m_i)_E \quad \forall i \in \{2, \dots, n_k\}, \tag{4.17}$$

and conditions in curly bracket in (2.7). If it's considered the j-th basis functions, for $j = 1, \dots, N^E_{\text{dof}}$, the previous equality yields to the matrix equation

$$\mathbf{G}^E_k \mathbf{\Pi}^{\nabla}_{E,k} = \mathbf{B}^E_k, \tag{4.18}$$

as detailed in the following. The first matrix $\mathbf{G}^E_k \in \mathbb{R}^{n_k \times n_k}$ derives from the stiffness matrix of monomials $\hat{\mathbf{G}}^E_k \in \mathbb{R}^{n_k \times n_k}$ defined as:

$$\left(\hat{\mathbf{G}}^E_k\right)_{ij} := (\nabla m_i, \nabla m_j)_E = \int_E \frac{\partial m_i}{\partial x}\frac{\partial m_j}{\partial x} + \int_E \frac{\partial m_i}{\partial y}\frac{\partial m_j}{\partial y} \quad \forall i, j \in \{1, \dots, n_k\}.$$

At this point, the matrices defined in the Subsection 4.2.1 come into play. The Vandermonde matrices of derivatives (4.15) and the diagonal quadrature weights matrix (4.7) are used :

$$\hat{\mathbf{G}}^E_k = (\mathbf{V}^E_{k,x})^T \mathbf{W}^E \mathbf{V}^E_{k,x} + (\mathbf{V}^E_{k,y})^T \mathbf{W}^E \mathbf{V}^E_{k,y}.$$

This matrix is singular, since its first row is full of zeros: this derives from the fact that the first column of either $\mathbf{V}^E_{k,x}, \mathbf{V}^E_{k,y}$ is null. Conditions in curly bracket in (2.7) fills this row, and new matrices are defined. Easily, integrals of each monomials on the boundary (if $k = 1$) or on E (if $k > 1$) are computed using, respectively, (4.8)-(4.9) or (4.5)-(4.6). Finally, matrix $\mathbf{G}^E_k$ involved in (4.18) is defined

$$\mathbf{G}^E_k := \hat{\mathbf{G}}^E_k + \begin{bmatrix} (\mathbf{w}^{\partial E})^T \mathbf{V}^{\partial E}_k \\ \mathbf{0} \in \mathbb{R}^{(n_k-1)\times n_k} \end{bmatrix} \quad \text{if } k = 1,$$

$$\mathbf{G}^E_k := \hat{\mathbf{G}}^E_k + \begin{bmatrix} (\mathbf{w}^{E})^T \mathbf{V}^{E}_k \\ \mathbf{0} \in \mathbb{R}^{(n_k-1)\times n_k} \end{bmatrix} \quad \text{if } k > 1.$$

As in the first case, the second matrix $\mathbf{B}^E_k \in \mathbb{R}^{n_k \times N^E_{\text{dof}}}$ needs a preliminary matrix to be defined. The matrix containing in column j the right hand side of (4.17) computed for the j-th basis function is denoted with $\hat{\mathbf{B}}^E_k \in \mathbb{R}^{n_k \times N^E_{\text{dof}}}$, i.e. for all $j \in \{1, \dots, N^E_{\text{dof}}\}$ and $i \in \{1, \dots, n_k\}$

$$\left(\hat{\mathbf{B}}^E_k\right)_{ij} := (\nabla \varphi_j, \nabla m_i)_E = \left(\varphi_j, \frac{\partial m_i}{\partial \hat{\mathbf{n}}}\right)_{\partial E} - (\varphi_j, \Delta m_i)_E, \tag{4.19}$$

using the Green's formula. The first term of right hand side of (4.19) is non-zero for the boundary basis functions (4.1), whereas the second one is non-zero for the internal basis functions (4.2). Two matrices are created to collect these values:

- $\hat{\mathbf{B}}_k^{\partial E} \in \mathbb{R}^{n_k \times N_{\text{dof}}^{\partial E}}$ collects the values of the first term. As already remarked, only boundary basis functions φ^∂ are involved. Here arise the importance of taking Gauss-Lobatto quadrature nodes as DOFs on the edges: since $\varphi^\partial, j = 1, \dots, N_{\text{dof}}^{\partial E}$, is part of a Lagrangian basis, the integral $\left(\varphi_j, \frac{\partial m_i}{\partial \hat{\mathbf{n}}}\right)_E$ is computed exactly using the value of the normal derivative at the correspondent quadrature node, i.e.,

$$\left(\hat{\mathbf{B}}_k^{\partial E}\right)_{ij} := \left(\varphi_j, \frac{\partial m_i}{\partial \hat{\mathbf{n}}}\right)_E = (\mathbf{w}^{\partial E})_j \frac{\partial m_i}{\partial \hat{\mathbf{n}}}(x_j^{\partial E}), \quad j \in \{1, \dots, N_{\mathcal{Q}}^{\partial E}\},$$

where the quadrature weights vector (4.9) is used. Basically, using (4.8) and (4.10)

$$\hat{\mathbf{B}}_k^{\partial E} = (\hat{\mathbf{V}}_{k,x}^{\partial E})^T \mathbf{W}_x^{\partial E} + (\hat{\mathbf{V}}_{k,y}^{\partial E})^T \mathbf{W}_y^{\partial E}.$$

- $\hat{\mathbf{B}}_k^{\circ E} \in \mathbb{R}^{n_k \times N_{\text{dof}}^{\circ}}$ collects the values of the second term. As already remarked, only internal basis functions φ° are involved. Then, since $\Delta m_i \in \mathbb{P}_{k-2}(E)$ and using the definition (4.16),

$$\begin{aligned} -\left(\hat{\mathbf{B}}_k^{\circ E}\right)_{ij} &= (\varphi_j^\circ, \Delta m_i)_E = \sum_{l=1}^{n_{k-2}} (\varphi_j^\circ, (\mathbf{L}_E^k)_{li} m_l)_E = \sum_{l=1}^{n_{k-2}} (\mathbf{L}_E^k)_{li} (\varphi_j^\circ, m_l)_E \\ &\overset{(4.2)}{=} \sum_{l=1}^{n_{k-2}} |E| (\mathbf{L}_E^k)_{li} \delta_{lj} = |E| (\mathbf{L}_E^k)_{ji}, \quad i \in \{1, \dots, n_k\}, j \in \{1, \dots, N_{\text{dof}}^{\circ}\}. \end{aligned}$$

Basically

$$\hat{\mathbf{B}}_k^{\circ E} = -|E| \left[(\mathbf{L}_E^k)_{1 \dots N_{\text{dof}}^{\circ}; 1 \dots n_k} \right]^T.$$

From (4.19), it's possible to derive the following relation thanks to the previous matrix list:

$$\hat{\mathbf{B}}_k^E = \begin{pmatrix} \hat{\mathbf{B}}_k^{\partial E} & \hat{\mathbf{B}}_k^{\circ E} \end{pmatrix}.$$

Notice that the elements of the first row of $\hat{\mathbf{B}}_k^E$ are all zeros by definition (4.19). To add the closing condition, if $k = 1$, the integral of basis functions on E must be computed. Since the basis functions are Lagrangian at the quadrature points, their integrals on the boundary equal the quadrature weights in the corresponding points. If $k > 1$, the integrals of all basis functions on the polygon are involved. Since these functions are Lagrangian on the element with respect to the DOFs, the integral is always zero except for the first internal basis function, whose integral equals $|E|$ (see (4.2)). Finally, the matrix $\mathbf{B}_E^k$ is defined such that:

$$\mathbf{B}_k^E := \hat{\mathbf{B}}_k^E + \begin{bmatrix} (\mathbf{w}^{\partial E})^T \\ \mathbf{0} \in \mathbb{R}^{(n_k - 1) \times N_{\text{dof}}^E} \end{bmatrix} \quad \text{if } k = 1,$$

$$\mathbf{B}_k^E := \hat{\mathbf{B}}_k^E + \begin{bmatrix} \mathbf{0} \in \mathbb{R}^{N_{\text{dof}}^{\partial E}} & |E| & \mathbf{0} \in \mathbb{R}^{n_{k-2}-1} \\ & \mathbf{0} \in \mathbb{R}^{(n_k - 1) \times N_{\text{dof}}^E} & \end{bmatrix} \quad \text{if } k > 1.$$

At the end, the matrix $\mathbf{\Pi}_{E,k}^\nabla$ representing the H^1-orthogonal projection is built using (4.18).

The second projector is the L^2- projection $\Pi^0_{E,k-1}(\cdot)$ defined in (2.13) using k instead of $k-1$. As before, using the set of monomials (2.1) as a basis for $\mathbb{P}_{k-1}(E)$, an equation similar to (4.17) is obtained:

$$\sum_{j=1}^{n_{k-1}} (m_j, m_i)_E \left(\mathrm{dof}_{\mathbb{P}_{k-1}(E)}(\Pi^0_{E,k-1}(\varphi))\right)_j = (\varphi, m_i)_E, \quad \forall i \in \{1, \dots, n_{k-1}\}, \tag{4.20}$$

where φ are the basis functions of $V_{k,\delta}(E)$. This equality clearly suggests the creation of a mass matrix of monomials $\mathbf{H}^E_k \in \mathbb{R}^{n_k \times n_k}$ such that:

$$\left(\mathbf{H}^E_k\right)_{ij} := (m_i, m_j)_E, \quad \forall i,j \in \{1, \dots, n_k\} \implies \mathbf{H}^E_k = (\mathbf{V}^E_k)^T \mathbf{W}^E \mathbf{V}^E_k, \tag{4.21}$$

where preliminary matrices (4.5), (4.7) are used.

Now, the right hand side of (4.20) must be computed. The columns of the new matrix $\mathbf{C}^E_{k-1} \in \mathbb{R}^{n_{k-1} \times N^E_{\mathrm{dof}}}$ contains these values, for each basis function against all monomials in $\mathcal{M}_{k-1}(E)$.
If $k = 1$, the property of the VEM space $V_{k,\delta}(E)$ (2.6) is used:

$$(\varphi_j, 1)_E = (\Pi^\nabla_{E,k}(\varphi_j), 1)_E, \quad j = 1,2,3 \implies \mathbf{C}^E_0 = \left(\left(\mathbf{H}^E_1\right)_{1;1,2,3}\right)\mathbf{\Pi}^\nabla_{E,1}.$$

If $k > 1$, using (4.1) and (4.2) follows directly that

$$\mathbf{C}^E_{k-1} := \begin{bmatrix} \mathbf{0} \in \mathbb{R}^{n_{k-2} \times N^{\partial E}_{\mathrm{dof}}} & |E|\mathbf{I} \in \mathbb{R}^{n_{k-2} \times n_{k-2}} \\ (\mathbf{H}^E_k)_{n_{k-2}+1,\dots,n_{k-1};1,\dots,n_k} \mathbf{\Pi}^\nabla_{E,k}. & \end{bmatrix}$$

Finally, the matrix $\mathbf{\Pi}^0_{E,k-1} \in \mathbb{R}^{n_{k-1} \times N^E_{\mathrm{dof}}}$ representing the operator $\Pi^0_{E,k-1}(\cdot)$ is obtained from the linear system:

$$\mathbf{H}^E_{k-1} \mathbf{\Pi}^0_{E,k-1} = \mathbf{C}^E_{k-1}. \tag{4.22}$$

The last projectors are $\Pi^0_{E,k-1}\frac{\partial}{\partial x}, \Pi^0_{E,k-1}\frac{\partial}{\partial y} : V_{k,\delta}(E) \to P_{k-1}(E)$, such that, $\forall v_\delta \in V_{k,\delta}(E)$,

$$\begin{aligned} \left(\Pi^0_{E,k-1}\frac{\partial v_\delta}{\partial x}, p\right)_E &= \left(\frac{\partial v_\delta}{\partial x}, p\right)_E \quad \forall p \in \mathbb{P}_{k-1}(E), \\ \left(\Pi^0_{E,k-1}\frac{\partial v_\delta}{\partial y}, p\right)_E &= \left(\frac{\partial v_\delta}{\partial y}, p\right)_E \quad \forall p \in \mathbb{P}_{k-1}(E). \end{aligned} \tag{4.23}$$

Let us define

$$\Pi^0_{E,k-1}\nabla v_\delta := \begin{bmatrix} \Pi^0_{E,k-1}\frac{\partial v_\delta}{\partial x} \\ \Pi^0_{E,k-1}\frac{\partial v_\delta}{\partial y} \end{bmatrix}.$$

Following the VEM philosophy, since the derivative of basis functions are unknown, the projection of derivatives are computed directly. The matrix $\mathbf{H}^E_{k-1}$ defined (4.21) is involved as mass matrix in both (4.23); the right hand sides requires the computation of integrals of all basis functions (2.5) against monomials in $\mathcal{M}_{k-1}(E)$. These are collected in two new matrices

$$\mathbf{E}^E_{k-1,x}, \mathbf{E}^E_{k-1,y} \in \mathbb{R}^{n_{k-1} \times N^E_{\mathrm{dof}}}, \tag{4.24}$$

whose computation is proposed later. Once these matrices are built, the matrices $\mathbf{\Pi}^{0,x}_{E,k-1}, \mathbf{\Pi}^{0,y}_{E,k-1} \in \mathbb{R}^{n_{k-1} \times N^E_{\text{dof}}}$ representing $\Pi^0_{E,k-1}\frac{\partial}{\partial x}, \Pi^0_{E,k-1}\frac{\partial}{\partial y}$ are obtained as follows:

$$\mathbf{H}^E_{k-1}\mathbf{\Pi}^{0,*}_{E,k-1} = \mathbf{E}^E_{k-1,*}, \quad * \in \{ x, y \}.$$

Finally, let's construct the matrices (4.24). Consider the first equality in (4.23) and apply Green's theorem:

$$\left(\frac{\partial \varphi}{\partial x}, m\right)_E = \sum_{e \text{ edge of } E} (\varphi, m\hat{n}_{e,x})_e - \left(\varphi, \frac{\partial m}{\partial x}\right)_E \quad \forall m \in \mathcal{M}_{k-1}(E).$$

Since basis functions belongs to $\mathbb{P}_k(\partial E)$, the first scalar product is the integral of a polynomial of degree $2k-1$ on the boundary of E, then it can be computed exactly thanks to the use of the values of φ and m at the Gauss-Lobatto quadrature points on the boundary, similarly to the case involved in Proposition 1. Using (4.5), (4.11) and (4.12), then $\forall j \in \{1, \dots, N^{\partial E}_{\text{dof}}\}$ and $\forall i \in \{1, \dots, n_{k-1}\}$,

$$\begin{aligned}\left(\varphi^\partial_j, m_i\hat{n}_{\partial E,x}\right)_{\partial E} &= \sum_{l=1}^{N^{\partial E}_{\text{dof}}} (\mathbf{w}^{\partial E}_x)_l m_i(x^{\partial E}_l)\varphi^\partial_j(x^{\partial E}_l) \overset{(4.1)}{=} \sum_{l=1}^{N^{\partial E}_{\text{dof}}} (\mathbf{w}^{\partial E}_x)_l m_i(x^{\partial E}_l)\varphi_j(x^{\partial E}_l) \\ &= (\mathbf{w}^{\partial E}_x)_j m_i(x^{\partial E}_j) = \left(\mathbf{W}^{\partial E}_x\right)_{jj}\left(\mathbf{V}^E_{k-1}\right)_{ji} = \left(\mathbf{V}^E_{k-1}\right)^T_{:i}\left(\mathbf{W}^{\partial E}_x\right)_{:j}.\end{aligned}$$

The second scalar product is non zero for φ° only, and, since $\frac{\partial m}{\partial x} \in \mathbb{P}_{k-2}(E)$, it's a multiple of one of internal DOFs, defined as the moments with respect to monomials in $\mathcal{M}_k(E)$. Using (4.13)

$$\begin{aligned}\left(\varphi^\circ_j, \frac{\partial m_i}{\partial x}\right)_E &= \sum_{l=1}^{n_{k-2}} \left(\varphi^\circ_j, (\mathbf{D}^E_{k,x})_{li} m_l\right)_E \overset{(4.2)}{=} \sum_{l=1}^{N_{k-2}} (\mathbf{D}^E_{k,x})_{li}|E|\delta_{jl} \\ &= |E|\left(\mathbf{D}^E_{k,x}\right)_{ji} \quad \forall i \in \{1, \dots, N_{k-1}\}, j \in \{1, \dots, N^\circ_{\text{dof}}\}.\end{aligned}$$

In conclusion, thanks to (4.8), (4.12), the desired matrix is obtained

$$\mathbf{E}^E_{k-1,x} := \left[(\mathbf{V}^{\partial E}_{k-1})^T\mathbf{W}^{\partial E}_x \quad -|E|\left[(\mathbf{D}^E_{k,x})_{1,\dots,N^\circ_{\text{dof}};1,\dots,n_{k-1}}\right]^T\right].$$

Similarly, using (4.14) instead of (4.13),

$$\mathbf{E}^E_{k-1,y} := \left[(\mathbf{V}^{\partial E}_{k-1})^T\mathbf{W}^{\partial E}_y \quad -|E|\left[(\mathbf{D}^E_{k,y})_{1,\dots,N^\circ_{\text{dof}};1,\dots,n_{k-1}}\right]^T\right].$$

4.2.3 Local discrete system

This subsection is dedicated to the construction of the local VEM stiffness matrix of the element $E \in \tau_{i,\delta}$, related to the local discrete bilinear form (2.17). The creation of the first term of this form is performed using matrices $\mathbf{\Pi}^{0,x}_{E,k-1}, \mathbf{\Pi}^{0,y}_{E,k-1}$ of Subsection 4.2.2 and (4.7):

$$\mathbf{A}^C_{k,E} := \sum_{*=x,y} \left(\mathbf{\Pi}^{0,*}_{E,k-1}\right)^T \mathbf{W}^E \mathbf{\Pi}^{0,*}_{E,k-1} \in \mathbb{R}^{N^E_{\text{dof}} \times N^E_{\text{dof}}}. \tag{4.25}$$

In order to build the VEM stabilization matrix to implement (2.16), for each basis function φ_i, the DOFs of $\Pi^{\nabla}_{E,k}(\varphi_i)$ must be computed. In Subsection 4.2.2 the matrix $\mathbf{\Pi}^{\nabla}_{E,k}$ is described, whose columns contain the values of the DOFs of the H^1-projection of basis functions with respect to the monomial basis. To obtain the DOFs with respect to the VEM basis, a new matrix is introduced: $\mathbf{D}^E_k \in \mathbb{R}^{N^E_{\text{dof}} \times n_k}$ such that

$$(\mathbf{D}^E_k)_{ij} := \text{dof}_i(m_j) \quad \forall i \in \{1, \dots, N^E_{\text{dof}}\}, j \in \{1, \dots, n_k\}.$$

using (2.4). Clearly,

$$\mathbf{D}^E_k = \begin{bmatrix} \mathbf{V}^{\partial E}_k \\ \left(\frac{1}{|E|}\mathbf{H}^E_k\right)_{1,\dots,n_{k-2};1,\dots,n_k} \end{bmatrix}.$$

This matrix is used to obtain the stabilization matrix $\mathbf{A}^S_{E,k} \in \mathbb{R}^{N^E_{\text{dof}} \times N^E_{\text{dof}}}$, preliminarily defining

$$\mathbf{\Pi}^{\nabla,\text{dof}}_{E,k} := \mathbf{D}^E_k \mathbf{\Pi}^{\nabla}_{E,k} \in \mathbb{R}^{N^E_{\text{dof}} \times N^E_{\text{dof}}}.$$

Then, the matrix is obtained as follows:

$$\mathbf{A}^S_{E,k} = \|\mu\|_{L^\infty(E)} \left(\mathbf{I} - \mathbf{\Pi}^{\nabla,\text{dof}}_{E,k}\right)^T \left(\mathbf{I} - \mathbf{\Pi}^{\nabla,\text{dof}}_{E,k}\right), \tag{4.26}$$

where $\mathbf{I}$ is the $\mathbb{R}^{N^E_{\text{dof}} \times N^E_{\text{dof}}}$ identity matrix. The local stiffness matrix of the element E is computed using (4.25) and (4.26)

$$\mathbf{A}_{E,k} := \mathbf{A}^C_{E,k} + \mathbf{A}^S_{E,k}.$$

Regarding the right hand side of the first matrix equation of (4.3), the local contribution $\mathbf{b}_{E,k} \in \mathbb{R}^{N^E_{\text{dof}}}$ is computed by building the vector $\mathbf{f}_E \in \mathbb{R}^{N^E_{\mathcal{Q}}}$ containing the values of the forcing term at the internal quadrature points $\mathcal{Q}(E)$, by

$$\mathbf{b}_{E,k} = \left(\mathbf{V}^E_{k-1}\mathbf{\Pi}^0_{E,k-1}\right)^T \mathbf{W}^E \mathbf{f}_E. \tag{4.27}$$

It has been used (4.5), (4.7) and (4.22).

4.3 Numerical results for a benchmark problem

In this section, the use of the previously defined method on a DFN made up 3 fractures with $\mathcal{S} = \mathcal{S}_M$ is described and analyzed. In this case, the exact solution is known, and this allows to compare the obtained results, showing optimal convergence for the primal variable. In spite of being a simple network, the DFN showed in Figure 4.3 presents two geometrical peculiarities: a trace intersection and a trace tip. The second one is clearly visible also in Figure 4.2: the mesh creation process plans to extend the trace, reaching the closest edge of the triangulation. A rapid comparison between *base mesh* and *VEM mesh* highlights this fact.
Geometrically, the network is $\Omega = F_1 \cup F_2 \cup F_3$, where

$$\begin{aligned} F_1 &= \{(x, y, z) \in \mathbb{R}^3 : -1 \le x \le 1/2,\ -1 \le y \le 1,\ z = 0\}, \\ F_2 &= \{(x, y, z) \in \mathbb{R}^3 : -1 \le x \le 0,\ y = 0,\ -1 \le z \le 1\}, \\ F_3 &= \{(x, y, z) \in \mathbb{R}^3 : x = -1/2,\ -1 \le y \le 1,\ -1 \le z \le 1\}, \end{aligned}$$

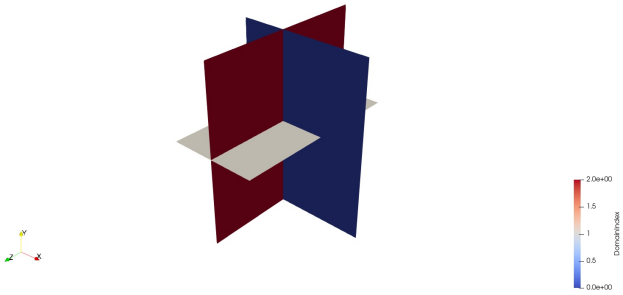

Figure 4.3: Geometry of the network composed by 3 fractures

with traces

$$S_1 = F_1 \cap F_2 = \{(x, y, z) \in \mathbb{R}^3 : -1 \leq x \leq 1/2,\ y = 0,\ z = 0\},$$
$$S_2 = F_1 \cap F_3 = \{(x, y, z) \in \mathbb{R}^3 : x = -1/2,\ -1 \leq y \leq 1,\ z = 0\},$$
$$S_3 = F_2 \cap F_3 = \{(x, y, z) \in \mathbb{R}^3 : x = -1/2,\ y = 0,\ -1 \leq z \leq 1\}.$$

Non-homogeneous Dirichlet boundary conditions on the whole boundary $\partial\Omega$ are imposed, and a load term on each fracture is calculated in such a way that the exact solution is given by:

$$H_1(x, y) = \frac{1}{10}\left(-x - \frac{1}{2}\right)\left(8xy\,(x^2 + y^2)\ \text{arctan2}(y, x) + x^3\right),$$
$$H_2(x, z) = \frac{1}{10}\left(-x - \frac{1}{2}\right)x^3 - \frac{4}{5}\,\pi\left(-x - \frac{1}{2}\right)x^3|z|,$$
$$H_3(y, z) = (y - 1)y(y + 1)(z - 1)z,$$

where $\text{arctan2}(y, x)$ is the four quadrant inverse tangent function with 2 arguments, that returns the appropriate quadrant of the computed angle y/x.

To present convergence results, it is noted that, since the values of the discrete solution are not explicitly known within the elements but only at the set of degrees of freedom, the errors are calculated by projecting the discrete solution onto the space of polynomials of degree k, as is customary in the VEM framework [7, 10]. The absolute errors are calculated as follows

$$(Err^H_{L^2})^2 = \sum_{E \in \tau_\delta} \|H - \Pi^\nabla_{E,k} h_E\|^2_{L^2(E)}, \tag{4.28}$$
$$(Err^H_{H^1})^2 = \sum_{E \in \tau_\delta} \|H - \Pi^\nabla_{E,k} h_E\|^2_{H^1(E)}, \tag{4.29}$$

where $\tau_\delta = \cup_{i=1}^N \tau_{\delta,i}$, $\Pi^\nabla_{E,k}$ is the projection operator of order k as defined in Section 2.1, H is the exact solution and h_E is the discrete solution restricted to element E. Regarding the absolute errors of approximation of Λ, defined in (1.8), two different norms are used: the first one is (3.20), and the second one

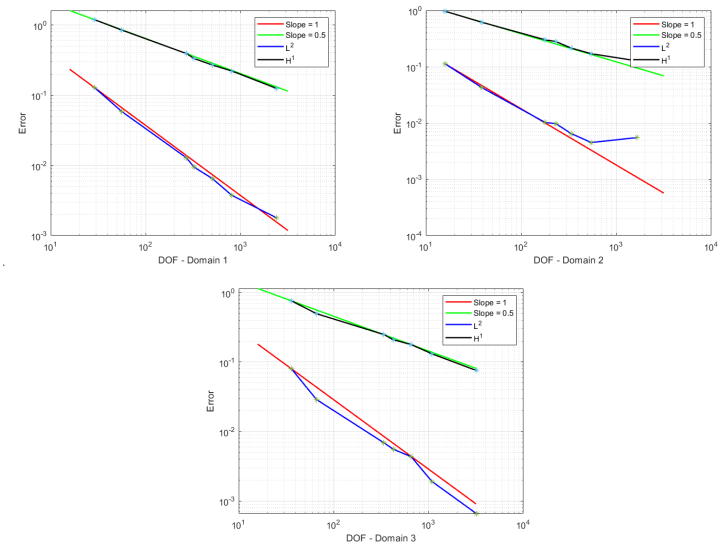

Figure 4.4: Convergence curves for the benchmark problem.

is now introduced.

$$(Err^{\Lambda}_{L^2})^2 = \sum_{S\in\mathcal{S}}\sum_{e\subset S} \|\Lambda - \lambda\|^2_e,$$
$$\left(Err^{\Lambda}_{H^{-\frac{1}{2}}}\right)^2 = \sum_{S\in\mathcal{S}}\sum_{e\subset S} |e|\,\|\Lambda - \lambda\|^2_e,$$

where Λ is the exact solution and λ is its discrete approximation. The thesis author commits to reporting the behavior of the approximation error of the flow calculated in these two ways in a future work. Instead, the convergence results for (4.28) and (4.29) are presented in Figure 4.4: here, the errors are plot versus the number of DOFS on the respective domain. In these simulation, $k = 1$ and the selected Mortar basis is M^1_h, defined in Section 3.1. Posthumous studies will include also convergence curves for different combinations of order k for the VEM space and of the type of the Mortar basis. Note the quite good agreement between the computed and the expected rates presented in [10]. Observe how there is an increase in the absolute error specifically at fracture F_1, which is the mortar domain on interface S_1, shared between F_0 and F_1, and the non-mortar domain on interface S_3, shared between F_1 and F_2. This change may be responsible for this behavior, and it will also be the subject of future studies.
In Table 4.1, Table 4.2, Table 4.3, some data emerged from simulations are showed: in particular, for every domain (whose *DomainIndex* is presented in Figure 4.3), are included the number of cells of the *VEM mesh*, the number of *internal dofs* of h , the number of *boundary dofs* of h, the number of total dofs and the two different discretization error of h.
Finally, the results obtained for the hydraulic head on the fractures are presented in Figure 4.5. A comparison with the recently cited article shows that the obtained results are correct.

NumCell2Ds	Dofs	Dirichlets	Total	$Err^H_{L^2}$	$Err^H_{H^1}$
59	29	20	49	1.28E-01	1.20E+00
117	56	30	86	5.87E-02	8.52E-01
532	269	58	327	1.28E-02	3.93E-01
648	324	66	390	9.44E-03	3.35E-01
1012	505	88	593	6.49E-03	2.70E-01
1636	812	113	925	3.73E-03	2.22E-01
4824	2395	208	2603	1.79E-03	1.25E-02

Table 4.1: $DomainIndex = 0$.

NumCell2Ds	Dofs	Dirichlets	Total	$Err^H_{L^2}$	$Err^H_{H^1}$
42	16	16	32	1.12E-01	9.67E-01
85	39	24	63	4.23E-02	6.16E-01
359	179	48	227	1.02E-02	3.02E-01
468	233	54	287	9.70E-03	2.80E-01
679	336	77	413	6.50E-03	2.15E-01
1102	547	96	643	4.50E-03	1.70E-01
3330	1659	184	1843	5.51E-03	1.27E-01

Table 4.2: $DomainIndex = 1$.

NumCell2Ds	Dofs	Dirichlets	Total	$Err^H_{L^2}$	$Err^H_{H^1}$
83	36	22	58	7.98E-02	7.61E-01
146	66	32	98	2.89E-02	4.97E-01
680	337	64	401	6.91E-03	2.50E-01
850	427	68	495	5.54E-03	2.10E-01
1318	657	95	752	4.33E-03	1.79E-01
2174	1086	125	1211	1.91E-03	1.32E-01
6394	3187	240	3427	6.59E-04	7.59E-02

Table 4.3: $DomainIndex = 2$.

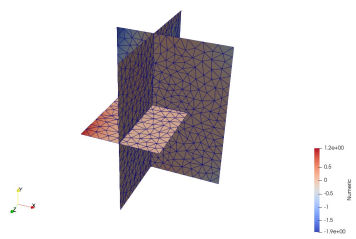

(a) *Solution on the whole domain.*

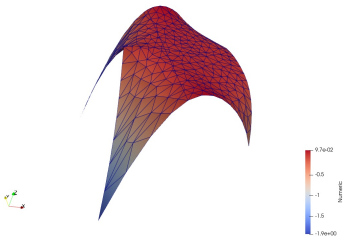

(b) *Computed hydraulic head h on fracture F_1.*

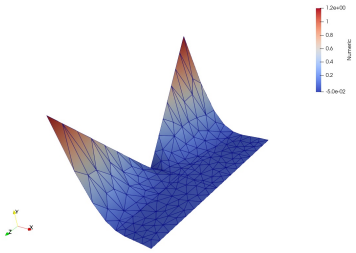

(c) *Computed hydraulic head h on fracture F_2.*

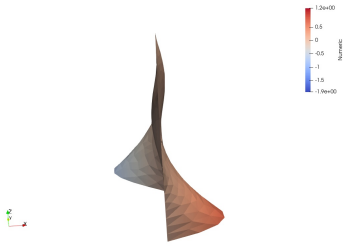

(d) *Computed hydraulic head h on fracture F_3.*

Figure 4.5: Numerical simulation of the solution across the DNF.

Conclusions

This master's thesis addresses and analyzes a numerical solution method for simulating fluid flow and transport phenomena in rock formations. The Discrete Fracture Network (DFN) method provides the geometric and mathematical foundation, with a focus on selecting an appropriate domain discretization method. Part of this work involved studying, comparing, and ultimately mixing the Virtual Element Method (VEM) and Mortar method. The ease of the mesh generation process is supported by the flexibility of virtual elements, which can handle meshes composed of elements in a wide variety of polygonal shapes. The Mortar approach takes advantage of the presence of subdomains to select a discretization method best suited to the local behavior of the partial differential equation solution being approximated. The choice of method can be made either a priori or a posteriori, independently of the discretization applied to adjacent subdomains. The hybrid VEM-Mortar formulation allows both of these advantages to be exploited and requires only weak continuity for the hydraulic head at fracture intersections.

The aim of this work was to study, at least from a theoretical perspective, a method positioned between the full VEM and hybrid VEM-Mortar approaches. This investigation led to significant findings: the a priori convergence estimate and the well-posedness of the problem open up possibilities for a numerical study of this new approach. As mentioned in the introduction, future research will allow for an in-depth examination of the numerical behavior of the solution based on the number of traces (*VEM* or *Mortar traces*) selected during domain discretization.

To lay the groundwork for this future research, it was challenging to adapt an existing C++ code—originally developed for a full VEM discretization—to the hybrid VEM-Mortar method and test it on a benchmark problem. The close alignment with results found in the literature demonstrates the potential to apply this work to more complex DFN models and to the newly introduced method. Here, particular attention will be given to error convergence rates and the conditioning of the saddle-point matrix.

Bibliography

[1] Pierre M. Adler and Jean-François Thovert. *Fractures and Fracture Networks*. Springer, 1999.

[2] B. Ahmad, A. Alsaedi, F. Brezzi, L.D. Marini, and A. Russo. Equivalent projectors for virtual element methods. *Computers & Mathematics with Applications*, 66(3):376–391, 2013.

[3] P. F. Antonietti, L. Beirao da Veiga, D. Mora, and M. Verani. A stream virtual element formulation of the stokes problem on polygonal meshes. *SIAM Journal on Numerical Analysis*, 52(1):386–404, 2014.

[4] L. Beirão da Veiga, Carlo Lovadina, and Alessandro Russo. Stability analysis for the virtual element method. *Mathematical Models and Methods in Applied Sciences*, 27(13):2557–2594, 2017.

[5] L Beirão da Veiga, Franco Brezzi, Andrea Cangiani, Gianmarco Manzini, L Donatella Marini, and Alessandro Russo. Basic principles of virtual element methods. *Mathematical Models and Methods in Applied Sciences*, 23(01):199–214, 2013.

[6] L Beirão da Veiga, Franco Brezzi, Luisa Donatella Marini, and Alessandro Russo. The hitchhiker's guide to the virtual element method. *Mathematical models and methods in applied sciences*, 24(08):1541–1573, 2014.

[7] L Beirão da Veiga, Franco Brezzi, Luisa Donatella Marini, and Alessandro Russo. Virtual element method for general second-order elliptic problems on polygonal meshes. *Mathematical Models and Methods in Applied Sciences*, 26(04):729–750, 2016.

[8] Lourenço Beirão Da Veiga, Franco Brezzi, L. Donatella Marini, and Alessandro Russo. The virtual element method. *Acta Numerica*, 32:123–202, 2023.

[9] Faker Ben Belgacem. Belgacem, f.b.: The mortar finite element method with lagrange multipliers. numer. math. 84(2), 173-197. *Numerische Mathematik*, 84:173–197, 12 1999.

[10] Matías Fernando Benedetto, Stefano Berrone, Andrea Borio, Sandra Pieraccini, and Stefano Scialo. A hybrid mortar virtual element method for discrete fracture network simulations. *Journal of Computational Physics*, 306:148–166, 2016.

[11] Matías Fernando Benedetto, Stefano Berrone, Sandra Pieraccini, and Stefano Scialò. The virtual element method for discrete fracture network simulations. *Computer Methods in Applied Mechanics and Engineering*, 280:135–156, 2014.

[12] Matías Fernando Benedetto, Stefano Berrone, and Stefano Scialò. A globally conforming method for solving flow in discrete fracture networks using the virtual element method. *Finite Elements in Analysis and Design*, 109:23–36, 2016.

[13] C. Bernardi, Y. Maday, and A. Patera. A new nonconforming approach to domain decomposition: the mortar element method. *Brezis, H.(ed.) et al., Nonlinear partial differential equations and their applications. Collège de France Seminar, volume XI. Lectures presented at the weekly seminar on applied mathematics, Paris, France,*, 1989.

[14] C. Bernardi, Y. Maday, and A. T. Patera. *Domain Decomposition by the Mortar Element Method*, pages 269–286. Springer Netherlands, Dordrecht, 1993.

[15] Christine Bernardi, Yvon Maday, and Francesca Rapetti. Basics and some applications of the mortar element method. *GAMM-Mitteilungen*, 28, 11 2005.

[16] F. Brezzi. On the existence, uniqueness and approximation of saddle-point problems arising from lagrangian multipliers. *Publications mathématiques et informatique de Rennes*, 8(S4):1–26, 1974.

[17] Franco Brezzi and L. Donatella Marini. Virtual element methods for plate bending problems. *Computer Methods in Applied Mechanics and Engineering*, 253:455–462, 2013.

[18] L. Beirao da Veiga, F. Brezzi, and L. D. Marini. Virtual elements for linear elasticity problems. *SIAM Journal on Numerical Analysis*, 51(2):794–812, 2013.

[19] L. Beirao da Veiga, C. Lovadina, and G. Vacca. Virtual elements for the navier–stokes problem on polygonal meshes. *SIAM Journal on Numerical Analysis*, 56(3):1210–1242, 2018.

[20] L. Beirao da Veiga, Carlo Lovadina, and Alessandro Russo. Stability analysis for the virtual element method, 2016.

[21] Maksymilian Dryja. A neumann-neumann algorithm for a mortar discretization of elliptic problems with discontinuous coefficients. *Numer. Math.*, 99(4):645–656, feb 2005.

[22] Jane CS Long, JS Remer, CR Wilson, and PA Witherspoon. Porous media equivalents for networks of discontinuous fractures. *Water resources research*, 18(3):645–658, 1982.

[23] Leszek Marcinkowski. Domain decomposition methods for mortar finite element discretizations of plate problems. *SIAM Journal on Numerical Analysis*, 39(4):1097–1114, 2002.

[24] Gergina Pencheva and Ivan Yotov. Balancing domain decomposition for mortar mixed finite element methods. *Numerical Linear Algebra with Applications*, 10, 2003.

[25] P. A. Raviart and J. M. Thomas. Primal hybrid finite element methods for 2nd order elliptic equations. *Mathematics of Computation*, 31(138):391–413, 1977.

[26] Dan Stefanica. Parallel feti algorithms for mortars. *Applied Numerical Mathematics*, 54(2):266–279, 2005. 6th IMACS.

[27] Andrea Toselli and Olof Widlund. *Domain Decomposition Methods – Algorithms and Theory*, volume 34. Springer International Publishing, 01 2005.

[28] Barbara Wohlmuth. Hierarchical a posteriori error estimators for mortar finite element methods with lagrange multipliers. *SIAM Journal on Numerical Analysis*, 36, 02 1999.

[29] Barbara Wohlmuth. *Discretization Methods and Iterative Solvers Based on Domain Decomposition*, volume 17. Springer, 01 2001.